Z. Phys. C – Particles and Fields 46, 93–109 (1990)

Zeitschrift für Physik C Particles and Fields

Exclusive semileptonic heavy meson decays including lepton mass effects

J.G. Körner[1] and G.A. Schuler[2,*]

[1] Institut für Physik, Universität, Staudinger Weg 7, D-6500 Mainz, Federal Republic of Germany
[2] II. Institut für Theoretische Physik, Universität, Luruper Chaussee 149, D-2000 Hamburg 50, Federal Republic of Germany

Received 10 August 1989

Abstract. We discuss the exclusive semi-leptonic (s.l.) bottom meson decays $B \to D(D^*) + l + \nu$ where we include non-zero lepton mass effects in the kinematics and dynamics. We develop the general formalism for the non-zero lepton mass case. We then look at how rates, spectra and angular correlations are affected by non-zero lepton masses in the context of a specific spectator quark model. Numerical results are presented for s.l. decays involving the e-, μ- and τ-leptons. We also discuss the s.l. decays $B \to \pi(\rho)$, $D \to K(K^*)$ and the free quark decay model.

1 Introduction

Recently the exclusive semileptonic (s.l.) decays of the bottom mesons $B \to D(D^*)$ and $B \to \pi(\rho)$ have attracted considerable attention in connection with the possible determination of the KM matrix elements V_{bc} and V_{bu} [1–5]. Most of the theoretical and experimental analyses of the exclusive s.l. decays have used the zero lepton mass approximation tacitly assuming that e.g. $m_\mu = 0$ is a good approximation for s.l. B-decays.

There is no doubt that one has to include lepton mass effects when one analyzes s.l. B-decays involving the τ-lepton. For the muonic decay modes one wants to make sure that the zero mass approximation is good especially in sensitive phase space regions as e.g. in the region of the lepton energy endpoint spectrum.

Two different aspects have to be considered when lepton mass effects are included in an analysis of s.l. decays. One is simply kinematical in that the kinematics of the decay processes change. The second aspect is of dynamical nature: When the lepton acquire mass one probes the scalar (or time-component) hadronic current form factor which is not accessible in the zero lepton mass case in addition to the 3-vector (or space-component) current form factors also measurable in the lepton mass zero case.

The present paper is structured such that in the first part we study the model independent kinematical and "spin-kinematical" aspects of s.l. decays involving massive leptons (Sects. 2, 3 and Appendices A, B). In the second part we turn to model specific predictions (Sects. 4, 5, 6).

In Sect. 2 we define invariant and helicity form factors. In Sect. 3 we derive differential decay rate formulae including azimuthal and polar lepton–hadron correlation effects. Section 3 also contains the corresponding angular distribution formula for the sequential decay $B \to D^*(\to D\pi) + W^-_{\text{off-shell}}$. In Sect. 4 we discuss the free quark decay (FQD) model. We calculate the FQD helicity amplitudes, which, when squared and summed, lead to the known rate formula. In Sect. 5 we introduce the spectator quark model of [4, 5] and derive analytical expressions for the invariant form factors including the new scalar form factor. Section 6 contains our numerical results. We calculate the various helicity rates defined in Sect. 3 for $B \to D(D^*)$, $B \to \pi(\rho)$, $D \to K(K^*)$ and the FQD model. Section 6 also contains a discussion of phase-space boundaries and how the Dalitz plot boundaries change when lepton mass effects are included. Section 7 contains a summary and our conclusions.

Some technical material is relegated to the appendices. Appendix A provides a brief synopsis of the decay kinematics. Appendix B contains a derivation of the angular lepton–hadron correlation functions presented in Sect. 3.

2 Invariant form factors and helicity form factors

We define invariant form factors by expanding the particle–particle current matrix elements along a standard set of covariants. One has

* Supported by Bundesministerium für Forschung und Technologie, 054HH 92P/3 Bonn, FRG

$$\langle D(p_2)|V_\mu|B(p_1)\rangle = T^D_\mu \tag{1a}$$

where

$$T^D_\mu = F^V_+(p_1+p_2)_\mu + F^V_- q_\mu \tag{1b}$$

and

$$\langle D^*(p_2)|A_\mu + V_\mu|B(p_1)\rangle = \varepsilon_2^{*\alpha} T^{D^*}_{\mu\alpha} \tag{2a}$$

where

$$T^{D^*}_{\mu\alpha} = F^A_1 g_{\mu\alpha} + F^A_2 p_{1\mu}p_{1\alpha} + F^A_3 q_\mu p_{1\alpha} + iF^V \varepsilon_{\mu\alpha\rho\sigma}p_1^\rho p_2^\sigma. \tag{2b}$$

$q_\mu = (p_1 - p_2)_\mu$ is the 4-momentum transfer. We have found it convenient to use the particle labels for the $J^{PC} = 0^{-+}$ and 1^{--} mesons involved in (1) and (2) instead of generic names. The invariants F^V_- and F^A_3 multiplying q_μ contribute only to the s.l. decays involving massive leptons since the corresponding lepton currents are conserved in the limit of vanishing lepton masses.

Next we calculate helicity form factors by taking the appropriate helicity projections of the covariants in (1) and (2). In order to make our conventions clear we shall explicate our covariant helicity projections. In the B rest frame with the z-axis along the $D(D^*)$ one has the current projections

$$\bar\varepsilon_\mu(\pm) = \frac{1}{\sqrt{2}}(0, \pm 1, -i, 0)$$

$$\bar\varepsilon_\mu(0) = \frac{1}{\sqrt{q^2}}(p, 0, 0, -q_0) \tag{3}$$

$$\bar\varepsilon_\mu(t) = \frac{1}{\sqrt{q^2}}(q_o, 0, 0, -p)$$

where q_o and p are the energy and momentum of the $W_{\text{off-shell}}$ in the B rest system. They are given by

$$2M_1 q_o = M_1^2 - M_2^2 + q^2$$
$$2M_1 p = (M_1^4 + M_2^4 + q^4 - 2M_1^2M_2^2 - 2M_1^2q^2 - 2M_2^2q^2)^{1/2}. \tag{4}$$

The bar over the polarization four-vectors in (3) reminds one of the fact that the quantization axis is along the negative current axis, i.e. $\bar\varepsilon_\mu = \varepsilon_\mu(\theta = \pi)$ [6].

In the following we shall refer to the helicity components of the currents in (3) as to the four helicities of the $W_{\text{off-shell}}$. Three of these are orthogonal to its momentum, i.e. $q^\mu \bar\varepsilon_\mu(m) = 0$ for $m = \pm, 0$, and thus make up the spin 1 part of the $W_{\text{off-shell}}$. The spin 0 (time-) component $m = t$ has the property $\bar\varepsilon_\mu(t) \propto q_\mu$ and clearly does not contribute to the s.l. decays in the lepton mass zero limit as mentioned above. The four helicity components have the orthonormality property

$$\bar\varepsilon^*_\mu(m)\bar\varepsilon^\mu(m') = g_{mm'} \quad (m, m' = t, \pm, 0). \tag{5}$$

and satisfy the completeness relation

$$\sum_{m,m'} \bar\varepsilon_\mu(m)\bar\varepsilon^*_\nu(m')g_{mm'} = g_{\mu\nu} \tag{6}$$

where $g_{mm'} = \text{diag}(+, -, -, -)$.

For the D^* (spin 1) one has

$$\varepsilon_{2\alpha}(\pm) = \mp\frac{1}{\sqrt{2}}(0, 1, \pm i, 0)$$

$$\varepsilon_{2\alpha}(0) = \frac{1}{M_2}(p, 0, 0, E_2) \tag{7}$$

where E_2 is the energy of the D^* in the B rest system

$$2M_1E_2 = M_1^2 + M_2^2 - q^2. \tag{8}$$

They satisfy the orthonormality condition

$$\varepsilon^*_{2\alpha}(m)\varepsilon^\alpha_2(m') = -\delta_{mm'} \tag{9}$$

and the completeness relation

$$\sum_{m,m'} \varepsilon_{2\alpha}(m)\varepsilon^*_{2\beta}(m')\delta_{mm'} = -g_{\alpha\beta} + \frac{p_{2\alpha}p_{2\beta}}{M_2^2}. \tag{10}$$

We can then project out the relevant helicity form factors from the invariant form factors (1) using the polarization vectors (3) and (7) valid for the B rest frame. One has

$$H^D_m = \bar\varepsilon^{*\mu}(m)T^D_\mu \quad m = t, 0 \tag{11}$$

where

$$H^D_o = \frac{2M_1p}{\sqrt{q^2}}F^V_+$$

$$H^D_t = \frac{1}{\sqrt{q^2}}((M_1^2 - M_2^2)F^V_+ + q^2F^V_-) \tag{12}$$

and

$$H^{D^*}_m = \varepsilon^{*\alpha}_2(m)\bar\varepsilon^{*\mu}(m)T^{D^*}_{\mu\alpha} \quad m = 0, \pm$$
$$H^{D^*}_t = \varepsilon^{*\alpha}_2(0)\bar\varepsilon^{*\mu}(t)T^{D^*}_{\mu\alpha} \tag{13}$$

where

$$H^{D^*}_o = \frac{1}{2M_2\sqrt{q^2}}((M_1^2 - M_2^2 - q^2)F^A_1 + 2M_1^2p^2F^A_2)$$

$$H^{D^*}_t = \frac{M_1p}{M_2\sqrt{q^2}}(F^A_1 + \tfrac{1}{2}(M_1^2 - M_2^2 + q^2)F^A_2 + q^2F^A_3)$$

$$H^{D^*}_\pm = F^A_1 \pm M_1pF^V. \tag{14}$$

We emphasize that the invariant and helicity form factors are functions of q^2 only.

3 Differential decay rates and angular distributions

Consider the angular decay distribution differential in the momentum transfer squared q^2. One has

$$\frac{d\Gamma}{dq^2 d\cos\theta d\chi} = \frac{G^2}{(2\pi)^4}|V_{bc}|^2\frac{(q^2 - \mu^2)p}{8M_1^2q^2}L_{\mu\nu}H^{\mu\nu} \tag{15}$$

where μ is the lepton mass, G is the Fermi coupling $G \cong 1.02\cdot 10^{-5}m_p^{-2}$ and V_{bc} is the (bc) Kobayashi–Maskawa matrix element. $L_{\mu\nu}$ is the lepton tensor build

from the current product of the left chiral lepton currents. In our normalization the lepton tensor is given by

$$L_{\mu\nu} = \tfrac{1}{8}\mathrm{Tr}\not{l}'+\mu\gamma_\mu(1-\gamma_5)\not{l}'\gamma_\nu(1-\gamma_5)$$
$$= l_\mu l'_\nu + l_\nu l'_\mu - \frac{q^2-\mu^2}{2}g_{\mu\nu} + i\varepsilon_{\mu\nu\alpha\beta}l^\alpha l'^\beta \qquad (16)$$

where $l(l')$ is the four-momentum of the lepton (antineutrino). Equation (16) refers to the case $(l^-\bar{\nu}_l)$. The corresponding lepton tensor for the case $(l^+\nu_l)$ is obtained from (16) by changing the sign of the ε-tensor contribution. We define our totally antisymmetric ε-tensor by $\varepsilon_{0123} = -1$. The hadron tensor $H_{\mu\nu}$ is given by the corresponding tensor product of the hadron currents defined in Sect. 2, i.e.

$$H_{\mu\nu} = \sum_{\text{spins}} \langle D(D^*)|j_\mu|B\rangle\langle D(D^*)|j_\nu|B\rangle^*$$
$$= \begin{cases} T^D_\mu (T^D_\nu)^* & B\to D \\ T^{D^*}_{\mu\alpha}(T^{D^*}_{\nu\beta})^*\left(-g^{\alpha\beta}+\dfrac{p_2^\alpha p_2^\beta}{M_2^2}\right) & B\to D^* \end{cases} \qquad (17)$$

In the one-hadron to one-hadron transition $B\to D(D^*)$ the rhs of (15) does not depend on the azimuthal angle χ. Using the results of Appendix B one obtains the $\cos\theta$ dependence

$$L_{\mu\nu}H^{\mu\nu} = \tfrac{2}{3}(q^2-\mu^2)$$
$$+\Big(\tfrac{3}{8}(1+\cos^2\theta)\hat{H}_U + \tfrac{3}{4}\sin^2\theta\hat{H}_L \pm \tfrac{3}{4}\cos\theta\hat{H}_P$$
$$+\frac{\mu^2}{2q^2}\left(\tfrac{3}{4}\sin^2\theta\hat{H}_U + \tfrac{3}{2}\cos^2\theta\hat{H}_L\right.$$
$$\left.+\tfrac{1}{2}\hat{H}_S + 3\cos\theta\hat{H}_{SL}\right)\Big) \qquad (18)$$

where we choose to define the polar angle θ to be the angle between the $D(D^*)$ and the lepton in the lepton–neutrino CM system as shown in Fig. 1. The upper and lower signs in front of the parity violating (p.v.) contribution $\hat{H}_P$ refer to the two cases $(l^-\bar{\nu}_l)$ and $(l^+\nu_l)$, respectively.

We have labelled the helicity components of the hadron tensor according to the standard notation used in describing the angular dependence of lepton–hadron correlations. In terms of the helicity amplitudes defined in Sect. 2 one has

i) spin 1 $\hat{H}_U = |H_+|^2 + |H_-|^2$ unpolarized-transverse
$\hat{H}_L = |H_o|^2$ longitudinal
$\hat{H}_P = |H_+|^2 - |H_-|^2$ parity-odd

for the spin 1 contributions. These are the helicity combinations that contribute also to the *on-shell* W^- decays. In addition, there are *off-shell* spin 0 contributions when lepton mass effects are included. These

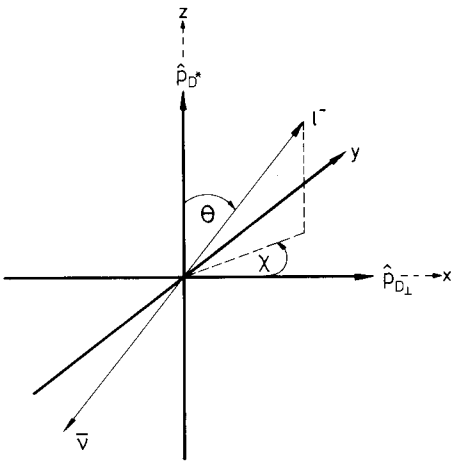

Fig. 1. Definition of the polar and azimuthal angles θ and χ of the lepton l^- in the $(l^-\bar{\nu}_l)$ CM frame. z-axis is along $\vec{P}_{D^*}$ and x-axis in the $(\vec{p}_{D^*}, \vec{p}_D)$ plane with $p_{Dx} \geqq 0$

are

ii) spin 0 $\hat{H}_S = 3|H_t|^2$ scalar
iii) spin 0 – spin 1 interference
$\hat{H}_{SL} = \mathrm{Re}(H_t H_o^*)$ scalar-longitudinal interference

We have separated (18) into lepton spin no-flip and flip contributions. The flip contribution brings in the characteristic flip factor $\mu^2/2q^2$ which vanishes in the zero lepton mass limit. The polar decay distribution (15, 18) agrees with the results of [7].

The lepton–hadron correlation function $L_{\mu\nu}H^{\mu\nu}$ reveals more structure when one considers current-induced one hadron to two hadron transitions as in the s.l. cascade decay $B\to D^*(\to D\pi)$. Now the azimuthal dependence in (15) becomes nontrivial.

One possible choice to describe the relative angular orientation of lepton and hadron frames is to define the angles θ and χ as in Fig. 1, where the z-axis is defined by the $D(D^*)$ momentum (helicity frame).* The x-axis provides the reference for the azimuthal measurement for which one needs a reference direction. In our case we define the x-axis to lie along the perpendicular component of the D-momentum in the decay chain $D^*\to D\pi$ as indicated in Fig. 1. It will become clear in a moment that the azimuthal measurement makes sense only in the s.l. $B\to D^*$ decay: although the weak nonleptonic cascade decay $D\to K\pi$ could establish an azimuthal reference axis also for the s.l. $B\to D$ decay, in principle, the azimuthal information cannot be conveyed to the decay $W^-_{\text{off-shell}}\to l^- + \bar{\nu}_l$ since the D has spin zero.

* Other choices of frames are of course possible as e.g. the transversity frame where the z-axis is chosen to lie perpendicular to the hadron plane. For example, we shall discuss the polar distribution in the transversity frame in Sect. 6. One should always keep one's mind open to different possible choices of frames which may be dictated by theoretical and/or experimental exigency

The hadron tensor now reads

$$H_{\mu\nu} = \langle (D^* \to) D\pi | j_\mu | 0 \rangle \langle (D^* \to) D\pi | j_\nu | 0 \rangle^* = H_{\mu\alpha;\nu\beta} Z^{\alpha\beta} B(D^* \to D\pi) = T^{D^*}_{\mu\alpha} (T^{D^*}_{\nu\beta})^* Z^{\alpha\beta} B(D^* \to D\pi) \quad (19)$$

where $B(D^* \to D\pi)$ is the branching ratio of $D^* \to D\pi$ and where $Z_{\alpha\beta}$ is the normalized decay tensor describing the strong decay $D^* \to D\pi$. It is given by

$$Z_{\alpha\beta} = \frac{3}{2} \frac{M_2^2}{(p_2 p_3)^2 - M_2^2 M_3^2} p_{3\alpha'} p_{3\beta'} S_{\alpha\alpha'}(p_2) S_{\beta\beta'}(p_2) \quad (20)$$

where p_3 and M_3 are the momentum and mass of the D and $S_{\alpha\alpha'}$ is the spin 1 propagator $S_{\alpha\alpha'}(p_2) = -g_{\alpha\alpha'} + p_{2\alpha} p_{2\alpha'}/M_2^2$. The decay tensor $Z_{\alpha\beta}$ is normalized according to

$$\int_0^{2\pi} d\chi^* \int_{-1}^{1} d\cos\theta^* Z_{\alpha\beta} = S_{\alpha\beta}(p_2) \quad (21)$$

where θ^* and χ^* are the polar and azimuthal angle of the D in the D^* rest system.

In writing down the general decay distribution of the cascade decay $B \to D^*(\to D\pi) l\nu$ we shall always use the narrow resonance approximation. The resulting decay distribution in thus four-fold. In addition to the variables θ, χ and q^2 introduced earlier we shall use the polar angle θ^* as the fourth variable. θ^* is defined as the polar angle between the D^* and D in the rest system of the D^*.

Using the results of Appendix B one obtains the full four-fold decay distribution

$$\begin{aligned}
&\frac{d\Gamma(B \to D^*(\to D\pi) l\nu)}{dq^2 \, d\cos\theta \, d\chi \, d\cos\theta^*} \\
&= B(D^* \to D\pi) \frac{1}{2\pi} \left[\tfrac{3}{8}(1 + \cos^2\theta) \tfrac{3}{4} \sin^2\theta^* \, d\Gamma_U/dq^2 \right. \\
&\quad + \tfrac{3}{4} \sin^2\theta \tfrac{3}{2} \cos^2\theta^* \, d\Gamma_L/dq^2 \\
&\quad - \tfrac{3}{4} \sin^2\theta \cos 2\chi \tfrac{3}{4} \sin^2\theta^* \, d\Gamma_T/dq^2 \\
&\quad - \tfrac{9}{16} \sin 2\theta \cos\chi \sin 2\theta^* \, d\Gamma_I/dq^2 \\
&\quad \pm \tfrac{3}{4} \cos\theta \tfrac{3}{4} \sin^2\theta^* \, d\Gamma_P/dq^2 \\
&\quad \mp \tfrac{9}{8} \sin\theta \cos\chi \sin 2\theta^* \, d\Gamma_A/dq^2 \\
&\quad + \tfrac{3}{4} \sin^2\theta \tfrac{3}{4} \sin^2\theta^* \, d\tilde{\Gamma}_U/dq^2 \\
&\quad + \tfrac{3}{2} \cos^2\theta \tfrac{3}{2} \cos^2\theta^* \, d\tilde{\Gamma}_L/dq^2 \\
&\quad + \tfrac{3}{4} \sin^2\theta \cos 2\chi \tfrac{3}{4} \sin^2\theta^* \, 2d\tilde{\Gamma}_T/dq^2 \\
&\quad + \tfrac{9}{8} \sin 2\theta \cos\chi \sin 2\theta^* \, d\tilde{\Gamma}_I/dq^2 \\
&\quad + \tfrac{3}{2} \cos^2\theta^* \tfrac{1}{2} d\tilde{\Gamma}_S/dq^2 \\
&\quad + 3 \cos\theta \tfrac{3}{2} \cos^2\theta^* \, d\tilde{\Gamma}_{SL}/dq^2 \\
&\quad \left. + \tfrac{9}{4} \sin\theta \cos\chi \sin 2\theta^* \, d\tilde{\Gamma}_{ST}/dq^2 \right]. \quad (22)
\end{aligned}$$

As in (18) the upper and lower signs in front of the p.v. contributions $d\Gamma_P$ and $d\Gamma_A$ again refer to the two cases $(l^- \bar{\nu}_l)$ and $(l^+ \nu_l)$, respectively.

We have found it convenient to define partial helicity rates $d\Gamma_i/dq^2$ and $d\tilde{\Gamma}_i/dq^2$ according to

$$\frac{d\Gamma_i}{dq^2} = \frac{G^2}{(2\pi)^3} |V_{bc}|^2 \frac{(q^2 - \mu^2)^2 p}{12 M_1^2 q^2} \hat{H}_i \quad i = U, L, T, I, P, A \quad (23)$$

and

$$\frac{d\tilde{\Gamma}_i}{dq^2} = \frac{\mu^2}{2q^2} \frac{d\Gamma_i}{dq^2} \quad i = U, L, T, I, P, A, S, SL, ST \quad (24)$$

where the partial rates $d\Gamma_i$ and $d\tilde{\Gamma}_i$ denote the lepton spin no-flip and flip contributions.

The reduced hadron tensor components $\hat{H}_i$ $(i = U, L, T, I, P, A, S, SL, ST)$ appearing in (23) and (24) are bilinear expressions of the four (two) helicity amplitudes $H_\pm^{D^*}, H_o^{D^*}$ and $H_t^{D^*}$ (H_o^D and H_t^D) describing the current-induced transitions $B \to D^*$ ($B \to D$) (see (12) and (14)). For $i = U, L, P, S$ and SL the relevant bilinear expressions $\hat{H}_i$ have already been listed after (18). The remaining four interference components are given by

spin 1: $\hat{H}_T = \mathrm{Re}(H_+ H_-^*)$
transverse interference

$\hat{H}_I = \frac{1}{2} \mathrm{Re}(H_+ H_o^* + H_- H_o^*)$
transverse-longitudinal interference

$\hat{H}_A = \frac{1}{2} \mathrm{Re}(H_+ H_o^* - H_- H_o^*)$
parity asymmetric

spin 0–spin 1 interference:

$\hat{H}_{ST} = \frac{1}{2} \mathrm{Re}(H_+ H_t^* + H_- H_t^*)$
scalar-transverse interference.

Since the available q^2-range $(q^2 \leqq (M_1 - M_2)^2)$ is below the physical threshold $q^2 = (M_1 + M_2)^2$, we have assumed throughout that the invariant and helicity form factors are real. Thus we dropped angular terms in (22) that depend on the phase differences of helicity amplitude, i.e. angular terms that are multiplied by coefficients $\mathrm{Im}(H_i H_j^*)$, $i \neq j$.*

When integrating (22) over $\cos\theta^*$ and χ one recovers the two-fold decay distribution resulting from (18) up to the branching ratio factor $B(D^* \to D\pi)$. Further integration over $\cos\theta$ yields the differential q^2-distribution

$$\frac{d\Gamma}{dq^2} = \frac{d\Gamma_{U+L}}{dq^2} + \frac{d\tilde{\Gamma}_{U+L}}{dq^2} + \frac{d\tilde{\Gamma}_S}{dq^2} \quad (25)$$

If one is interested in the differential lepton energy (E_l) and momentum (p_l) distribution, one needs to relate the dE_l, dp_l and $d\cos\theta$ differentials which can be obtained from differentiating (A4) and $E_l^2 - p_l^2 = \mu^2$.

* The corresponding observables represent T-odd observables the presence of which would signal true CP-violating effects if rescattering effects can be neglected as assumed in the above derivation

One has $E_l dE_l = p_l dp_l$ and

$$\frac{d\cos\theta}{dE_l} = -2q^2 \frac{1}{p(q^2-\mu^2)} \tag{26}$$

where E_l and p_l are the lepton's energy and momentum in the B rest frame.

Finally, integrating (25) over q^2 yields the total decay rate. The necessary q^2-integrations in the limits (A1) have to be done numerically.

4 Free quark decay model

Let us list the helicity amplitudes of the free quark decay model. One has

$$h^{\mathrm{FQD}}_{o,t} = \langle c\downarrow|J_{o,t}|b\downarrow\rangle = (\sqrt{Q_+} + \sqrt{Q_-})\frac{p+q_o}{\sqrt{q^2}}$$

$$h'^{\mathrm{FQD}}_{o(t)} = \langle c\uparrow|J_{o,t}|b\uparrow\rangle = -(+)(\sqrt{Q_+} - \sqrt{Q_-})\frac{\sqrt{q^2}}{p+q_0}$$

$$h^{\mathrm{FQD}}_{-(+)} = \langle c\downarrow(\uparrow)|J_{-(+)}|b\uparrow(\downarrow)\rangle$$
$$= \sqrt{2}(-(+)\sqrt{Q_+} - \sqrt{Q_-}) \tag{27}$$

where $Q_\pm = (m_1 \pm m_2)^2 - q^2$ with quark masses $m_b = m_1$ and $m_c = m_2$.

When one computes the longitudinal and time-like contributions to the reduced hadron tensor components $\hat{H}_L$, $\hat{H}_S$ and $\hat{H}_{SL}$ one has to sum over unprimed and primed helicity amplitudes, i.e. $\hat{H}_L = |h^{\mathrm{FQD}}_o|^2 + |h'^{\mathrm{FQD}}_o|^2$ etc. The reduced hadron tensor components in the FQD case are given by

$$\hat{H}_U = 8(m_1^2 + m_2^2 - q^2)$$

$$\hat{H}_L = 4\left(m_1^2 + m_2^2 - q^2 + \frac{4m_1^2p^2}{q^2}\right)$$

$$\hat{H}_P = \mp 16\, m_1 p$$

$$\hat{H}_S = 3\hat{H}_L$$

$$\hat{H}_{SL} = 8m_1 p \frac{m_1^2 - m_2^2}{q^2} \tag{28}$$

where the upper and lower signs in the p.v. contribution $\hat{H}_P$ in (28) refer to the quark and antiquark transition cases $q_1 \to q_2$ and $\bar{q}_1 \to \bar{q}_2$, respectively.

The q^2-spectrum is given by

$$\frac{d\Gamma}{dq^2} = \frac{1}{2}\frac{G^3}{(2\pi)^3}|V_{bc}|^2 \frac{(q^2-\mu^2)^2 p}{12m_1^2 q^2}$$
$$\cdot 4\left[3(m_1^2 + m_2^2 - q^2)\left(1 + \frac{\mu^2}{q^2}\right)\right.$$
$$\left. + \frac{4m_1^2p^2}{q^2}\left(1 + 2\frac{\mu^2}{q^2}\right)\right] \tag{29}$$

where one has to remember to include the statistical spin factor 1/2 when using the general rate formula (25).

The total rate, finally, is obtained from (29) by q^2-integration where the relevant q^2-range is given by (A1). The integration can in fact be done analytically and results in a somewhat lengthy closed-form expression given e.g. in [8]. Numerical results for the FQD model will be presented in Sect. 6.

5 Spectator quark model

Let us briefly recall the spectator quark model approach of [4, 5] that was used to calculate the invariant and helicity form factors of the current induced s.l. $B \to D(D^*)$ transitions. The particle helicity amplitudes were matched to the free quark decay helicity amplitudes at $q^2 = 0$, assuming that the spectator quark is spin-inert. Thus one has

$$H_o^{D,D^*} = \langle D, D^*|J_o|B\rangle \cong \tfrac{1}{2} I_{bc}\langle c\downarrow|J_o|b\downarrow\rangle,$$
$$H^{D^*}_{-(+)} = \langle D^*\downarrow(\uparrow)|J_{-(+)}|B\rangle$$
$$\cong \frac{1}{\sqrt{2}} I_{bc}\langle c\downarrow(\uparrow)|J_{-(+)}|b\downarrow(\uparrow)\rangle. \tag{30}$$

The factors $\frac{1}{2}(1/\sqrt{2})$ are spin projection factors and I_{bc} is to be interpreted as the $B \to D(D^*)$ wave function overlap. It is the same for the D and D^* since the D and D^* have the same spatial properties in the quark model. In the equal mass case charge normalization fixes $I = 1$. In the unequal mass situation $m_b \gg m_c$ one expects incomplete overlap between the B and $D(D^*)$ wave functions leading to $I_{bc} < 1$. This is due to the fact that the light spectator quark's low momentum does not match with the energetic c-quark coming from the weak $b \to c$ decay when they are collected in the $D(D^*)$ wave function. In order to be definite we take $I_{bc} = 0.7$ for the wave function overlap mismatch factor I_{bc} as e.g. estimated in [2] for the $b \to c$ transitions.

The matching conditions (30) can be solved for the invariant form factors F_+^V, F_1^A, F_2^A and F^V that contribute in the lepton mass zero limit. We identity $m_b = M_B = M_1$ and $m_c = M_D\,(\approx M_{D^*}) = M_2$. One obtains

$$F_+^V(0) = I_{bc}$$

$$F_1^A(0) = (M_1 + M_2) I_{bc}$$

$$F_2^A(0) = \frac{-2}{(M_1 + M_2)} I_{bc}$$

$$F^V(0) = F_2^A(0). \tag{31}$$

The matching solutions (31) holds for the semi-leptonic $B(b) \to D(c)$, $D^*(c)$ and $D(c) \to K(s)$, $K^*(s)$ transitions. For the $B(\bar{b}) \to D^*(\bar{c})$ and $D(\bar{c}) \to K^*(\bar{s})$ transitions, $F^V(0)$ acquires an extra sign. Thus, from (14), one has the relations $H^\pm\ (\bar{Q} \to \bar{q}) = H^\mp (Q \to q)$ for the transverse helicity amplitudes.

To obtain the matching solutions for the two form factors F_-^V $(B \to D)$ and F_3^A $(B \to D^*)$ that multiply q_μ (see (1) and (2)) requires the solution of the matching conditions (30) and the corresponding ones for the time-component helicity amplitudes to the next order in q^2.

For the time-like and longitudinal components one now has

$$H_o^{D(D^*)} = \langle D(D^*)|J_o|B\rangle$$
$$\cong \tfrac{1}{2} I_{bc}(\langle c\downarrow|J_o|b\downarrow\rangle + (-)\langle c\uparrow|J_o|b\uparrow\rangle)$$
$$H_t^{D(D^*)} = \langle D(D^*)|J_t|B\rangle$$
$$\cong \tfrac{1}{2} I_{bc}(\langle c\downarrow|J_t|b\downarrow\rangle + (-)\langle c\uparrow|J_t|b\uparrow\rangle). \quad (32)$$

The transverse matching conditions remain as in (30). Solving the matching conditions (32) and the transverse part of (30) to first order in q^2 one obtains the solutions (31) as well as the solutions for the two form factors multiplying q_μ at the same time. One has

$$F_-^V(0) = -\frac{M_1 - M_2}{M_1 + M_2} I_{bc}$$
$$F_3^A(0) = -F_2^A(0). \quad (33)$$

In obtaining the small q^2 solution of the matching conditions the invariant form factors have been held fixed at their $q^2 = 0$ values, i.e. their dynamical q^2-dependence was not included in the small q^2-expansion.

We would like to mention that one obtains the same $q^2 = 0$ form factor values as in (31) and (33) if one works with boosted quark model wave functions [9]. The solutions (31) and (33) can be obtained in a compact form by evaluating the corresponding quark model matrix elements at $q^2 = 0$, cif.

$$\langle D|V_\mu|B\rangle$$
$$= -\frac{I_{bc}}{2(M_1 + M_2)} \mathrm{Tr}\,\gamma_5(\not{p}_2 + M_2)\gamma_\mu\gamma_5(\not{p}_1 - M_1)$$
$$\langle D^*|V_\mu + A_\mu|B\rangle$$
$$= \frac{-I_{bc}}{2(M_1 + M_2)} \mathrm{Tr}\,\not{\epsilon}_2^*(\not{p}_2 + M_2)\gamma_\mu(1 - \gamma_5)\gamma_5(\not{p}_1 - M_1). \quad (34)$$

The invariant form factors (31) and (33) are continued to $q^2 \neq 0$ by using pole-type form factors with a power behaviour given by the QCD power counting rules.

The q^2-dependence of the form factors is fixed by nearest meson-dominance in the appropriate current channel with monopole behaviour (q^{-2}) for F_+^V, F_-^V and F_1^A and dipole behaviour (q^{-4}) for F_2^A, F^V and F_3^A according to the power counting rules of QCD [10]. For the sake of simplicity we work only with one effective meson $(b\bar{c})$ current mass, for which we take B_c^* (6.34 GeV). The spacing among the various $(b\bar{c})$ bound state levels is presumably so small that one effective mass value is sufficient to set the scale of the q^2-dependence in the range $0 \leqq q^2 \leqq (M_1 - M_2)^2$.

The q^2-dependence of our form factors is thus given by

$$F(q^2) = F(0)\cdot\left(\frac{m_{FF}^2}{m_{FF}^2 - q^2}\right)^n \quad (35)$$

where $n = 1$ for F_+^V, F_-^V and F_1^A, $n = 2$ for F_2^A, F_3^A and F^V and $m_{FF} = 6.34\,\mathrm{GeV}$.

The matching solutions (31) and (33) and the power behaved form factors (35) completely specify our model of $B \to D(D^*)$ semileptonic decays. For the sake of brevity we shall in the following refer to this model as the KS- (Körner–Schuler) model [5].

The matching solutions for the s.l. decays $B \to \pi(\rho)$ and $D \to K(K^*)$ discussed later on are obtained from (31) and (33) by the obvious replacements $I_{bc} \to I_{bu}, I_{cs}$ and $m_{FF}(b\bar{c}) \to m_{FF}(b\bar{u})$, $m_{FF}(c\bar{s})$, respectively.

6 Numerical results

In this section we present numerical results on the exclusive s.l. decays of bottom and charm mesons. Many models of exclusive s.l. heavy meson decays have been proposed in the last few years. Among these are [2–5, 7, 11–29]. An understanding of the dynamics of the s.l. decays will be eventually reached by a detailed comparison of the measured values of experimental observables such as rates, spectra, polarization and angular decay distributions with the predictions of the various models. In this paper we choose the spectator quark model of [5] (KS model) in order to highlight the qualitative features of expected rates, spectra, angular distributions and polarization observables. Although the KS model has successfully stood the first tests in the $b \to c$ sector it goes without saying that such a simple first generation model may have to undergo some fine tuning at a later stage when more data becomes available.

Our main discussion will be concerned with the s.l. decays $B \to D(D^*)$ since one expects to have numerous data on these decays in the next few years. We also present some results on the interesting yet suppressed exclusive s.l. decays $B \to \pi(\rho)$. We finally also proffer some numerical results for exclusive s.l. D-decays.

We start our discussion by presenting a Dalitz plot for the s.l. decay $\bar{B}^o \to D^{*+} + l^- + \bar{\nu}_l$ for $l = e, \mu, \tau$ in Fig. 2. There is only a small change in the phase space boundary going from the electron to the muon which occurs at the left lower corner at low q^2- and E_l-values, whereas there is no visible change at the right boundary curve. According to (A2) the maximal lepton energy is only shifted by $(m_\mu^2 - m_e^2)/2M_B$ which is invisible at the scale of the plot. We already anticipate from this fact that the lepton's energy or momentum endpoint spectrum is only changed insignificantly when going from the electron to the muon. Compared to the e- and μ-cases the τ phase space is considerably reduced and is shifted to larger values of q^2 and E_l.

Figure 3 shows the corresponding Dalitz plot for the s.l. decays $D^o \to K^{*-} + l^+ + \nu_l$. Now the reduction of phase space becomes more pronounced when going from the electron to the muon. At the scale of the plot there is, however, no visible shift on the right shoulder of the phase space boundary.

Next we turn our discussion to the partial helicity

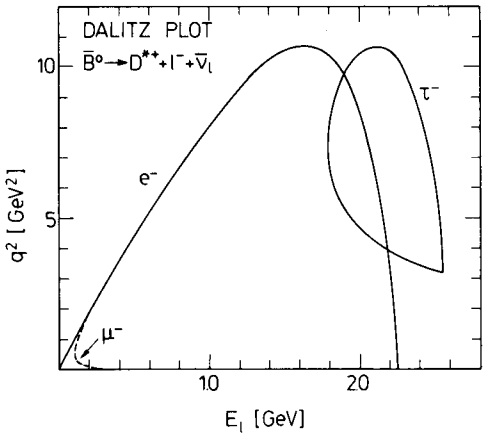

Fig. 2. Boundaries of physical region in (q^2, E_l)-Dalitz plot for $B^o \to D^{*+} + l^- + \bar{\nu}_l$ for $l = e, \mu, \tau$

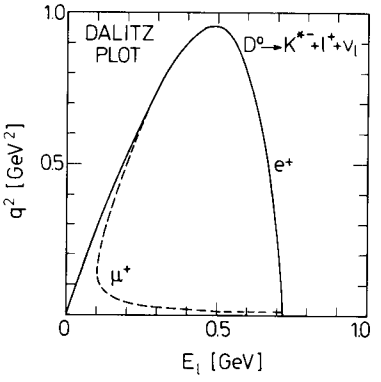

Fig. 3. Boundaries of physical region in (q^2, E_l)-Dalitz plot for $D^o \to K^{*-} + l^+ + \nu_l$ for $l = e, \mu$

rates $d\Gamma_i/dq^2$ (no-flip) and $d\tilde{\Gamma}_i/dq^2$ (flip) for the $b \to c$ transitions. It turns out to be convenient to discuss their q^2-dependence by first defining rescaled helicity form factors according to

lepton spin no-flip:

$$h_i = A(q^2) H_i \quad i = 0, +, - \tag{36}$$

lepton spin flip:

$$\tilde{h}_i = \sqrt{\mu^2/2q^2}\, A(q^2) H_i \quad i = 0, +, -$$
$$\tilde{h}_t = \sqrt{3}\sqrt{\mu^2/2q^2}\, A(q^2) H_t \tag{37}$$

where

$$A(q^2) = \frac{G}{4M_1} \frac{q^2 - \mu^2}{q^2} \sqrt{\frac{pq^2}{6\pi}} |V_{bc}|. \tag{38}$$

According to (25) the angle integrated differential q^2-rate is then given by

$$\frac{d\Gamma}{dq^2} = \sum_{0,+,-} |h_i|^2 + \sum_{t,0,+,-} |\tilde{h}_i|^2. \tag{39}$$

In Fig. 4. we plot the q^2-dependence of the rescaled helicity form factors h_i and $\tilde{h}_i$ for $B \to D$ in the e- and τ-modes. One notes that the longitudinal no-flip amplitude is considerably reduced at lower q^2-values going from e to τ. This reduction is due to the threshold like factor $(q^2 - \mu^2)/q^2$ appearing in the rescaled helicity amplitudes. The longitudinal flip amplitude $\tilde{h}_o$ is further reduced by the flip factor $\sqrt{\mu^2/2q^2}$. Quite remarkable is the large value of the time-like (or scalar) flip amplitude $\tilde{h}_t$. This can be traced to the fact that the scalar current contribution proceeds via an orbital s-wave and thus there is no pseudo-threshold factor (proportional to p) to temper the enhancement at large q^2 resulting from the time-like form factors in the helicity amplitudes (see (12) and [28]).

In Fig. 5 we show the q^2-dependence of the rescaled helicity amplitudes for $B \to D^*$ in the e- and τ-modes. The largest reduction in the no-flip amplitudes again occurs for the longitudinal no-flip amplitude h_o. Contrary to the $B \to D$ case, however, all flip amplitudes are generally quite small compared to the no-flip amplitudes. This can again be traced to the partial wave structure of the scalar current contribution which is now an orbital p-wave (see (14) and [28]).

Figures 4 and 5 also show the q^2-dependence of the rescaled helicity amplitudes $\tilde{h}_t$ for the τ-mode when the contribution of the scalar invariant form factors $F_-^V(q^2)$ and $F_3^A(q^2)$, respectively, are switched off. In the $B \to D$ case the contribution of $F_-(q^2)$ is destructive and consequently $\tilde{h}_t$ increases when $F_-^V(q^2)$ is switched off. The effect amounts to maximally $\cong 29\%$ at the amplitude level and maximally $\cong 66\%$ at the squared amplitude level. Since $|\tilde{h}_t|^2$ gives the dominant contribution to the rate, the above figures show that an accurate experimental determination of the s.l. $B \to D(\tau)$ rate alone would allow one to extract information on the sign and magnitude of the scalar invariant form factor $F_-^V(q^2)$. In the $B \to D^*$ case the contribution of the scalar form factor $F_3^A(q^2)$ to $\tilde{h}_t$ is constructive and consequently $\tilde{h}_t$ decreases when $F_3^A(q^2)$ is switched off. The effect is rather large ($\cong 50\%$ reduction over a wide q^2-range), however, on a small amplitude which would make an experimental determination of $F_3^A(q^2)$ from a rate measurement alone rather difficult.

In Fig. 6 we show the q^2-spectra for $B \to D(e, \tau)$ for the different helicity contributions defined in (23): Notable is the large reduction of the longitudinal no-flip contribution when one goes from the e- to the τ-case, whereas the scalar flip contribution $\tilde{S}$ dominates the differential rate over the whole accessible q^2-range.

Figure 7 shows the corresponding q^2-spectra for $B \to D^*(e, \tau)$. Since the lepton spin flip rates $d\Gamma_i/dq^2$ are quite small, they have not been included in the figure. The helicity rates appear to be uniformly reduced when going from the e- to the τ-case except for the longitudinal contribution which is disproportionally reduced because of the threshold-like factor $((q^2 - \mu^2)/q^2)^2$.*

* The threshold factor is also present in the e-case leading to the vanishing of $d\Gamma_L/dq^2$ at $q^2 = m_e^2$. However, this is not visible at the scale of Figs. 5 and 7

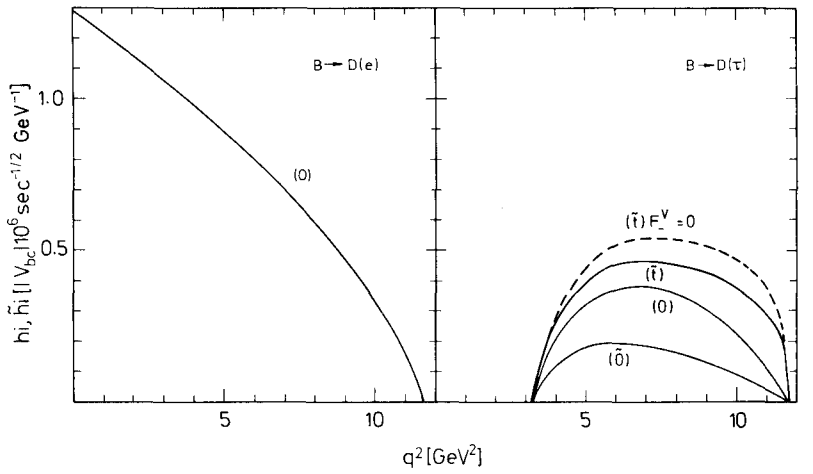

Fig. 4. Reduced helicity amplitudes h_i and $\tilde{h}_i$, $(i = t, 0)$ as functions of q^2 for $\overline{B^0} \to D^+ + e^- + \bar{\nu}_e$ (left) and $\overline{B^0} \to D^+ + \tau^- + \bar{\nu}_\tau$ (right). Also shown is $\tilde{h}_t$ with $F_-^V = 0$ (dashed curve)

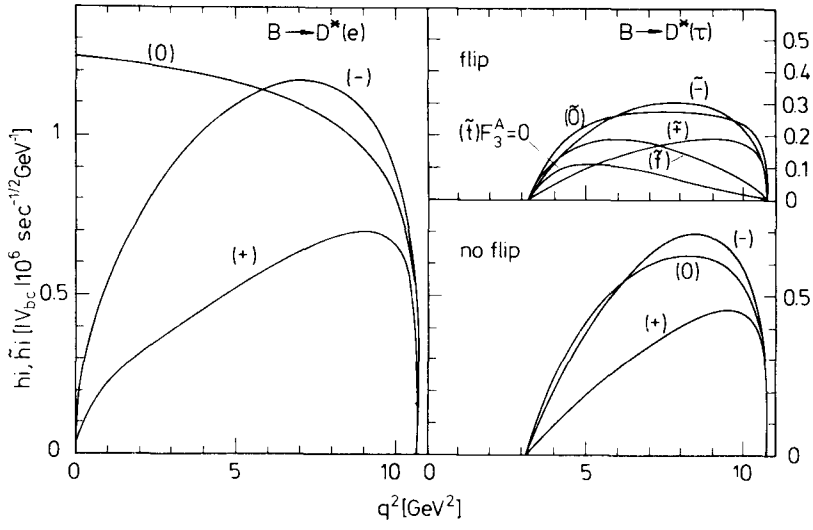

Fig. 5. Reduced helicity amplitudes h_i and $\tilde{h}_i$ $(i = t, +, -, 0)$ as functions of q^2 for $\overline{B^0} \to D^{*+} + e^- + \bar{\nu}_e$ (left) and $\overline{B^0} \to D^{*+} + \tau^- + \bar{\nu}_\tau$ (right). Also shown is $\tilde{h}_t$ with $F_3^A = 0$ (dashed curve)

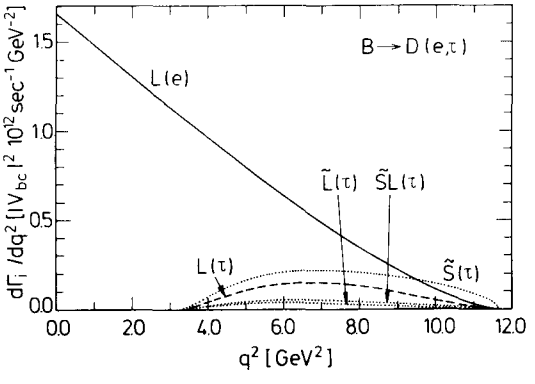

Fig. 6. Partial helicity rates $d\Gamma_i/dq^2$ and $d\tilde{\Gamma}_i/dq^2$ as functions of q^2 for $\overline{B^0} \to D^+ + l^- + \bar{\nu}_l$ with $l = e$ (full curve) and $l = \tau$ (dashed (no-flip) and dotted (flip))

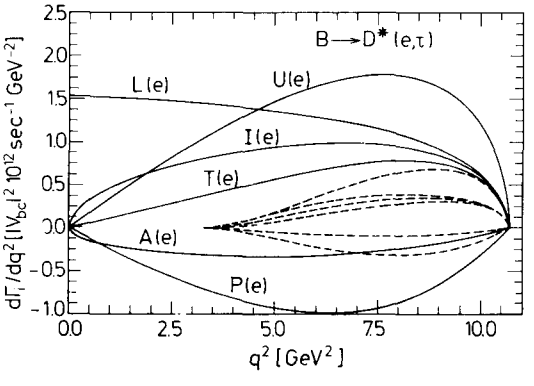

Fig. 7. Partial helicity rates $d\Gamma_i/dq^2$, $i = U, L, T, I, P, A$ as functions of q^2 for $\overline{B^0} \to D^{*+} + l^- + \bar{\nu}_l$ with $l = e$ (full curves) and $l = \tau$ (dashed curves). Flip rates $d\tilde{\Gamma}_i/dq^2$ are not shown as they are small on the scale of the figures. Labelling of dashed curves ($l = \tau$) is as labelling of full curves ($l = e$) from down (P) to up (U) at $q^2 = 7.5\,\mathrm{GeV}^2$

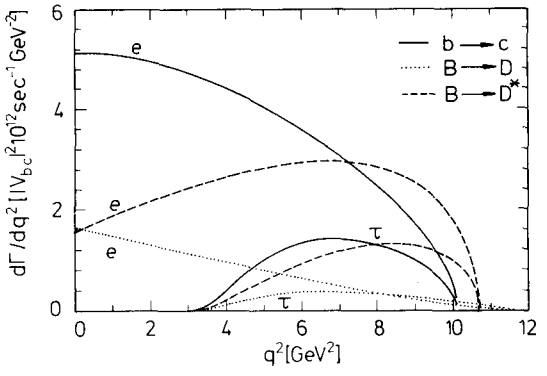

Fig. 8. q^2-spectrum of s.l. decay rates $\overline{B^0} \to D^+ + l^- + \bar{\nu}_l$ (dotted), $\overline{B^0} \to D^{*+} + l^- + \bar{\nu}_l$ (dashed) and $b \to c + l^- + \bar{\nu}_l$ (full) as functions of q^2 for $l = e, \tau$. The spectra of the τ-modes start at $q^2 = m_\tau^2$

In Figure 8 we show the total q^2-spectra $d\Gamma/dq^2 = d\Gamma_{U+L}/dq^2 + d\Gamma_{\tilde{U}+\tilde{L}}/dq^2 + d\Gamma_{\tilde{S}}/dq^2$ for the three s.l. decays $B \to D$, $B \to D^*$ and $b \to c$ in their e- and τ-modes. In the e-case the q^2-spectra decrease from their highest value at $q^2 = 0$ for $B \to D$ and $b \to c$, whereas there is a shoulder in the $B \to D^*$ spectrum at $q^2 = 7\,\mathrm{GeV}^2$ as also visible in the experimental $B \to D^*$ q^2-spectrum [30]. The q^2-spectra are uniformly reduced when going from the e-mode to the τ-mode for $B \to D^*$ and $b \to c$, whereas for $B \to D$ the τ-mode dominates over the e-mode for $q^2 \gtrsim 8\,\mathrm{GeV}^2$ contrary to the naive phase space expectations.

In Table 1 we have listed the partial helicity rates Γ_i and $\tilde{\Gamma}_i$ for the s.l. decays $B(b) \to D(c)$, $B(b) \to D^*(c)$ and $b \to c$ for the electron-, muon- and τ-cases. One notes that there are only slight changes in the decay rates going from the electron to the muon case. In the τ-mode all partial no-flip rates Γ_i are considerably reduced. The reduction is most pronounced for the longitudinal rates Γ_L as commented on already above.

The flip rates $\tilde{\Gamma}_i$ in the τ-mode are generally quite small compared to the total rate except for the S-wave enhanced scalar flip rate $\tilde{\Gamma}_S$ in the decay $B \to D$.

Going from the e- to the τ-mode the total rates are reduced to 26%, 25% and 18% for $B \to D$, $B \to D^*$ and the FQD $b \to c$, respectively. In the case of the decay $B \to D$ the strong suppression of the longitudinal no-flip contribution is made up by the strong scalar current excitation as explained above.

A measure of the flip/no-flip composition of the decay rate is given by the longitudinal polarization of the τ-lepton in the decay $W_{\text{off-shell}} \to \tau^- + \bar{\nu}_\tau$ in the $(\tau\bar{\nu}_\tau)$ CM frame. Since the massless τ-anti-neutrino has positive helicity the longitudinal τ-polarization is determined by*

$$P_L = \frac{d\tilde{\Gamma} - d\Gamma}{d\tilde{\Gamma} + d\Gamma}. \tag{40}$$

The average longitudinal polarization of the τ is then given by (we define $U := \Gamma_U$, $\tilde{U} := \tilde{\Gamma}_U$, etc.)

$$\langle P_L \rangle = \frac{\tilde{U} + \tilde{L} + \tilde{S} - U - L}{\tilde{U} + \tilde{L} + \tilde{S} + U + L}. \tag{41}$$

Using the numbers of Table 1 one finds $\langle P_L \rangle_{B \to D(\tau)} = 0.33$, $\langle P_L \rangle_{B \to D^*(\tau)} = -0.53$ and $\langle P_L \rangle_{b \to c(\tau)} = -0.26$. The average longitudinal polarization of the τ resulting from the decay $B \to D$ has undergone a drastic change from -1 in the lepton mass zero case to the large positive value of 0.33 due to the enhanced scalar current contribution $\tilde{\Gamma}_S$. It would be interesting to experimentally check on this prediction by analyzing the τ's subsequent decay distributions.

Concerning the ratio of total s.l. $B \to D$ and $B \to D^*$ rates we find the ratio of rates $R = \Gamma_{B \to D^*(e,\mu)}/\Gamma_{B \to D(e,\mu)}$

* Note that our quantization axis differs from the one used in [26] where the longitudinal polarization of the τ is calculated in the B-rest frame

Table 1. Partial rates, total rates and polarization parameters for s.l. $b \to c$ transitions in the e-, μ- and τ-sectors. We take $m_b = 4.73\,\mathrm{GeV}$, $m_c = 1.55\,\mathrm{GeV}$, $m_B = 5.28\,\mathrm{GeV}$, $m_{D^*} = 2.01\,\mathrm{GeV}$, $m_D = 1.865\,\mathrm{GeV}$ and $m_\tau = 1.8741\,\mathrm{GeV}$. Rates are in units of $|V_{bc}|^2\ 10^{12}\,\mathrm{s}^{-1}$

	$B \to D(e)$	$B \to D^*(e)$	$b \to c(e)$	$B - D(\mu)$	$B \to D^*(\mu)$	$b \to c(\mu)$	$B \to D(\tau)$	$B \to D^*(\tau)$	$b \to c(\tau)$
U	—	12.7	12.4	—	12.7	12.3	—	3.03	2.22
L	8.3	13.1	24.8	8.1	12.9	24.1	0.72	1.95	2.01
T	—	5.3	—	—	5.2	—	—	1.33	—
I	—	8.2	—	—	8.1	—	—	1.65	—
P	—	−6.9	−7.7	—	−6.9	−7.7	—	−1.39	−1.14
A	—	−2.6	—	—	−2.6	—	—	−0.42	—
$\tilde{U}$	—	—	—	—	0.02	0.02	—	0.64	0.51
$\tilde{L}$	—	—	—	0.04	0.04	0.12	0.17	0.43	0.49
$\tilde{T}$	—	—	—	—	0.01	—	—	0.28	—
$\tilde{I}$	—	—	—	—	0.01	—	—	0.35	—
$\tilde{S}$	—	—	—	0.13	0.12	0.36	1.26	0.46	1.47
$\tilde{S}L$	—	—	—	0.04	0.04	0.12	0.26	0.25	0.43
$\tilde{S}T$	—	—	—	—	0.01	—	—	0.20	—
Γ	8.3	25.8	37.2	8.27	25.7	36.9	2.15	6.50	6.72
$\langle P_L \rangle$	−1	−1	−1.	−0.95	−0.99	−0.97	0.33	−0.53	−0.26
α_{θ^*}	—	1.1	—	—	1.05	—	—	0.55	—

to be $R = 3.11$ which agrees with the recent experimental values $R = 3.0 \pm 1.6$ [31] and $1.6 \pm 0.8^{+0.7}_{-0.5}$ [32].

Different strategies can be adopted to experimentally separate the various angular coefficients $d\Gamma_i/dq^2$ and $d\tilde{\Gamma}_i/dq^2$ that appear in the angular expansion (22) (see also (23), (24)). Let us concentrate on the case $B \to D^*$ because of its rich angular structure.

A possible first strategy is to make a fit to the data using the angle functions appearing in (22). One would start with single angle distributions. Integrating (22) over θ and χ one arrives at

$$\frac{d\Gamma}{d\cos\theta^*} \propto \tfrac{3}{4}\sin^2\theta^*(U+\tilde{U}) + \tfrac{3}{2}\cos^2\theta^*(L+\tilde{L}) + \tfrac{3}{2}\cos^2\theta^*\tilde{S}. \tag{42}$$

Defining an asymmetry parameter α_{θ^*} from the angular distribution $W(\cos^2\theta^*) = 1 + \alpha_{\theta^*}\cos^2\theta^*$ one has

$$\alpha_{\theta^*} = \frac{-(U+\tilde{U}) + 2(L+\tilde{L}) + 2\tilde{S}}{U+\tilde{U}}. \tag{43}$$

From the partial rates in Table 1 one finds $\alpha_{\theta^*} = 1.1$ (0.55), where here, and in the following, the first quoted value stands for the e-mode and the value in the bracket stands for the τ-mode. The asymmetry value $\alpha_{\theta^*} = 1.1$ is in nice agreement with the ARGUS measurement [30]. The polarization of the D^* measured by the asymmetry parameter α_{θ^*} is considerably washed out in the τ-mode which can be traced to the strong suppression of the longitudinal rate L as explained before.

The polar $\cos\theta$ distribution is obtained from (22) by θ^* and χ integration. One has

$$\frac{d\Gamma}{d\cos\theta} \propto \tfrac{3}{8}(1+\cos^2\theta)U + \tfrac{3}{4}\sin^2\theta(L+\tilde{U}) + \tfrac{3}{4}\cos\theta(P+4\tilde{S}L) + \tfrac{3}{2}\cos^2\theta\tilde{L} + \tfrac{1}{2}\tilde{S}. \tag{44}$$

Defining asymmetry parameters by $W(\cos\theta) = 1 + \alpha'_\theta\cos\theta + \alpha_\theta\cos^2\theta$ has

$$\alpha'_\theta = \frac{2P + 8\tilde{S}L}{U + 2L + 2\tilde{U} + \frac{4}{3}\tilde{S}} \tag{45}$$

and

$$\alpha_\theta = \frac{U - 2L - 2\tilde{U} + 4\tilde{L}}{U + 2L + 2\tilde{U} + \frac{4}{3}\tilde{S}} \tag{46}$$

where we find $\alpha'_\theta = -0.35$ (-0.09) and $\alpha_\theta = -0.35$ (0.05). Note that the $\cos\theta$ contribution is quite small in the τ-mode due to a partial cancellation of the p.v. rate P and the parity conserving (p.c.) rate $\tilde{S}L$.

In the same vein one can define a polar angle distribution of the normal to the $(D^* \to D\pi)$ decay plane

$$\frac{d\Gamma}{d\cos\bar{\theta}} = 1 + \alpha_{\bar{\theta}}\cos^2\bar{\theta} \tag{48}$$

where $\bar{\theta}$ is the polar angle between the lepton momentum and the normal of the $(D^* \to D\pi)$ decay plane. Note that there is no linear $\cos\bar{\theta}$-term in (48). The asymmetry parameter $\alpha_{\bar{\theta}}$ is now given by

$$\alpha_{\bar{\theta}} = \frac{-\frac{1}{2}U + L + 3T + \tilde{U} - 2\tilde{L} - 6\tilde{T}}{\frac{3}{2}U + L - T + \tilde{U} + 2\tilde{L} + 2\tilde{T} + \frac{4}{3}\tilde{S}}. \tag{49}$$

Using the results of Table 1 one finds $\alpha_{\bar{\theta}} = 0.84$ (0.32). In the e-mode the asymmetry value is close to 1 which would also result from longitudinal (L) dominance in (49) as would be the case for the s.l. decay $B \to D$, with $D \to K\pi$ fixing the decay plane. In the τ-mode the asymmetry becomes smaller.

The asymmetry parameter $\alpha_{\bar{\theta}}$ is now also sensitive to the transverse interference contribution T. It is then a question of experimental exigency whether one attempts to determine T by the above polar measurement in the transversity frame or by an azimuthal measurement as discussed in the following.

The azimuthal χ-distribution finally is obtained by θ and θ^* integration. One has

$$\frac{d\Gamma}{d\chi} \propto U + \tilde{U} + L + \tilde{L} + \tilde{S} + \cos 2\chi\,(-T + 2\tilde{T}). \tag{50}$$

We define an azimuthal asymmetry parameter β by writing $W(\chi) = 1 + \beta\cos 2\chi$, where

$$\beta = \frac{-T + 2\tilde{T}}{U + \tilde{U} + L + \tilde{L} + \tilde{S}}. \tag{51}$$

We find $\beta = -0.21$ (-0.12).

A second strategy is to define suitable asymmetry ratios that project out the partial rates from (22). Let us consider the following four asymmetry ratios which project out the contributions of the p.c. partial rates Γ_T and Γ_I, and the p.v. partial rates Γ_P and Γ_A in the lepton mass zero limit. One has

$$T: A_T = \frac{d\Gamma(\chi) - d\Gamma(\chi+\pi/2) + d\Gamma(\chi+\pi) - d\Gamma(\chi+\frac{3}{2}\pi)}{d\Gamma(\chi) + d\Gamma(\chi+\pi/2) + d\Gamma(\chi+\pi) + d\Gamma(\chi+\frac{3}{2}\pi)} \qquad -\pi/4 \leqq \chi \leqq \pi/4 \tag{52}$$

$$I: A_I = N_I/D_I \tag{53}$$

with

$$\begin{aligned} N_I = {} & d\Gamma(\theta,\theta^*,\chi) - d\Gamma(\theta,\theta^*,\chi+\pi) \\ & - d\Gamma(\theta,\pi-\theta^*,\chi) + d\Gamma(\theta,\pi-\theta^*,\chi) \\ & - d\Gamma(\pi-\theta,\theta^*,\chi) + d\Gamma(\pi-\theta,\theta^*,\chi+\pi) \\ & + d\Gamma(\pi-\theta,\pi-\theta^*,\chi) \\ & - d(\pi-\theta,\pi-\theta^*,\chi+\pi) \end{aligned}$$

$$0 \leqq \theta^* \leqq \pi/2$$

$$\pi/2 \leqq \theta \leqq \pi$$

$$-\pi/2 \leqq \chi \leqq \pi/2$$

where the denominator D_I is given by the same expression with plus signs everywhere. We further define the asymmetries

$$P: A_{FB} = \frac{d\Gamma(\theta) - d\Gamma(\pi - \theta)}{d\Gamma(\theta) + d\Gamma(\pi - \theta)}$$

$$\frac{\pi}{2} \leqq \theta \leqq \pi \tag{54}$$

$$A: A_A = \frac{d\Gamma(\theta^*, \chi) - d\Gamma(\theta^*, \chi+\pi) - d\Gamma(\pi-\theta^*, \chi) + d\Gamma(\pi-\theta^*, \chi+\pi)}{d\Gamma(\theta^*, \chi) + d\Gamma(\theta^*, \chi+\pi) + d\Gamma(\pi-\theta^*, \chi) + d\Gamma(\pi-\theta^*, \chi+\pi)} \tag{55}$$

$$0 \leqq \theta^* \leqq \pi/2$$

$$-\pi/2 \leqq \chi \leqq \pi/2.$$

We have used a notation in (52–55) where the angles that do not appear in the arguments of the differential rate $d\Gamma$ in (52–55) have been integrated out over their physical ranges ($0 \leqq \theta, \theta^* \leqq \pi$, $0 \leqq \chi \leqq 2\pi$). Integrating over the remaining variables (numerator and denominator separately!) we finally obtain the following values for the asymmetry ratios in the KS model*

$$A_T = \frac{2}{\pi}\frac{-T + 2\tilde{T}}{\Gamma} = -0.13\ (-0.08) \tag{56}$$

$$A_I = \frac{2}{\pi}\frac{I - 2\tilde{I}}{\Gamma} = 0.20\ (0.09) \tag{57}$$

$$A_{FB} = -\frac{3}{4}\frac{P + 4\tilde{S}L}{\Gamma} = 0.20\ (0.05) \tag{58}$$

$$A_A = -\frac{3}{2}\frac{A - 2\tilde{S}T}{\Gamma} = 0.15\ (0.19). \tag{59}$$

One observes that the polarization type observables defined by the asymmetry parameters (52, 53, 54, 55) and the asymmetry ratios A_T, A_I and A_{FB} tend to become washed out when going from the e-mode to the τ-mode. In exception is the asymmetry ratio A_A which is stronger in the τ-mode.

In order to investigate the effect of the lepton mass on the lepton energy (E_l) and lepton momentum (p_l) spectra we have plotted the (E_l, p_l) spectra for the e-, μ- and τ-modes in Fig. 9 ($B \to D$) and Fig. 10 ($B \to D^*$). The lepton energy and momentum spectra for the e- and μ-modes practically fall on top of each other and are practically not discernible at the scale of Figs. 9 and 10. The energy threshold $E_l = \mu$ is barely visible in the E_l-spectrum of $B \to D(\mu)$ in Fig. 9 due to a relatively steep rise of the (E_l, p_l) spectra in the e-mode. In the τ-mode the p_l and E_l spectra are shifted to the left and to the right relative to the e- (and μ-) spectra, respectively, as one expects from the decay kinematics. The $B \to D$ spectra are somewhat softer than the $B \to D^*$ spectra for both the e- (and μ-) and τ-modes.

In order to highlight the shapes of the hadron and lepton momentum spectra we show the normalized hadron momentum and lepton momentum distributions as functions of the scaled hadron momentum $x = p/p_{\max}$ and scaled lepton momentum $y = p_l/p_{l\max}$ in Figs 11 and 12, respectively.

In Fig. 11 we show the $x(= p/p_{\max})$ hadron momentum spectrum of the s.l. decays $B \to D(e, \tau)$, $B \to D^*(e, \tau)$

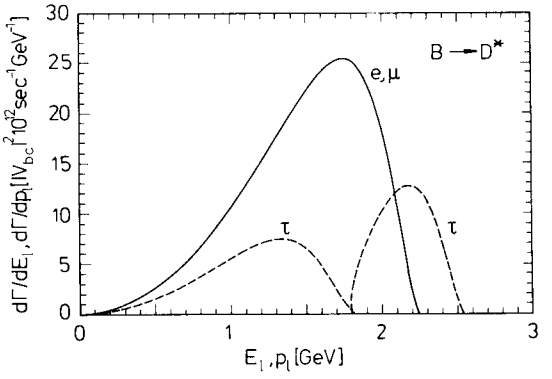

Fig. 9. Lepton energy E_l and lepton momentum p_l spectra for $\overline{B^0} \to D^+ + l^- + \bar{\nu}_l$ for $l = e, \mu$ (full and dotted) and $l = \tau$ (dashed). E_l and p_l spectra for e and μ practically lie on top of each other. Barely visible is E_μ spectrum at lower end

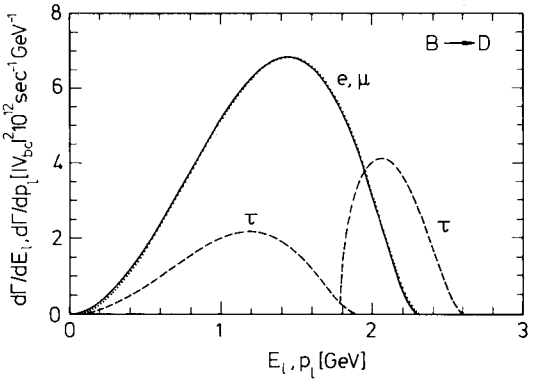

Fig. 10. Lepton energy E_l and lepton momentum p_l spectra for $\overline{B^0} \to D^{*+} + l^- + \bar{\nu}_l$ for $l = e, \mu$ (full) and $l = \tau$ (dashed). E_l and p_l spectra for e and μ are not resolvable at the scale of the figure

* Note that the forward–backward asymmetry A_{FB} and the asymmetry ratio A_A no longer test purely p.v. effects in the τ-mode

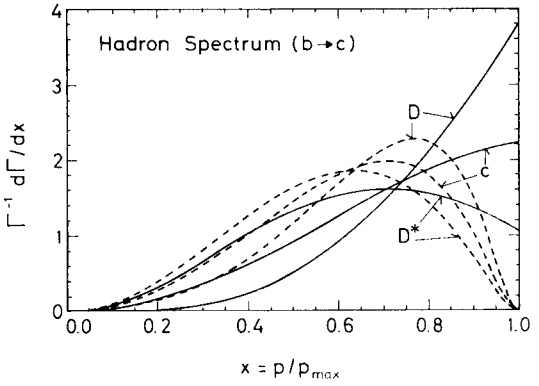

Fig. 11. $x\ (=p/p_{max})$ hadron momentum spectra of $b\to c(e)$ transitions (full lines) and $b\to c(\tau)$ (dashed lines)

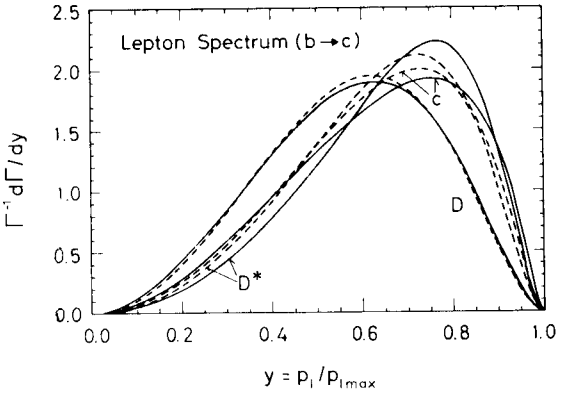

Fig. 12. $y\ (=p_l/p_{l\max})$ lepton momentum spectra of $b\to c(e)$ transitions (full lines) and $b\to c(\tau)$ transitions (dashed lines)

and $b\to c(e,\tau)$. In the e-mode the spectra rise to their highest values at $x=1$ for $B\to D$ and $b\to c$, whereas the $B\to D^*$ spectrum is softer and shows a shoulder around $x=0.6$ as also seen in the data [33]. In the τ-mode the heavy lepton kinematic forces the spectrum

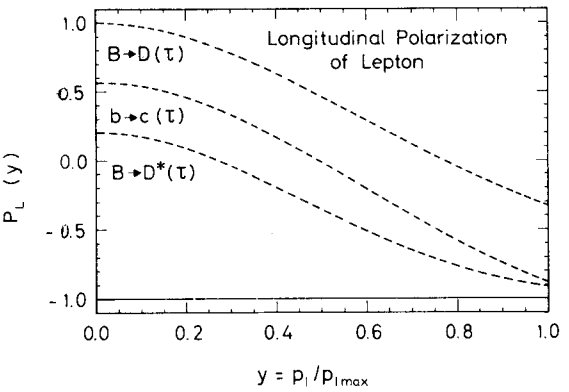

Fig. 13. $y\ (=p_l/p_{l\max})$ lepton momentum dependence of longitudinal polarization of the e and τ in $b\to c$ transitions

to go to zero at $x=1$. Consequently, the spectra become softer in the τ-modes. The same behaviour is observed to a lesser degree in the $y\ (=p_l/p_{l\max})$ lepton momentum spectra, where the spectra become slightly softer going from the e-mode to the τ-mode (see Fig. 12).

In Fig. 13 we show the y-behaviour of the longitudinal polarization $P_L(y)$ of the τ in the three decay modes $B\to D(\tau)$, $B\to D^*(\tau)$ and $b\to c(\tau)$ (in the e-mode the longitudinal polarization is obviously equal to 1).* In all three cases the longitudinal polarization decreases uniformly from its highest (positive) value at $y=0$ to its lowest (negative) value at $y=1$. That $P_L(y=0)=1$ for $B\to D$ is due to spin kinematics as there are only spin flip contributions to $B\to D$ in this limit. The longitudinal polarization of the τ is positive for the cases $B\to D^*$ and $b\to c$ close to $y=0$ where the

* We remind the reader that we are defining the longitudinal polarization of the τ relative to a z-direction determined by the τ three-momentum in the $(\tau\bar{\nu}_\tau)$ CM system

Table 2. Partial rates, total rates and polarization parameters for s.l. $b\to u$ transitions in the e-, μ- and τ-sectors. $m_b=4.73$ GeV and $m_u=0.3$ GeV. Rates in units of $|V_{bu}|^2 10^{12}\,s^{-1}$. Rates are for $\overline{B^0}\to\pi^+(\rho^+)$. Rates for $B^-\to\pi^0(\rho^0)$ are down by a factor 2. Also $\Gamma_{B^-\to\omega^0}\cong\frac{1}{2}\Gamma_{\overline{B^0}\to\rho^+}$ since $m_\omega\cong m_\rho$

	$B\to\pi(e)$	$B\to\rho(e)$	$b\to u(e)$	$B-\pi(\mu)$	$B\to\rho(\mu)$	$b\to u(\mu)$	$B\to\pi(\tau)$	$B\to\rho(\tau)$	$b\to u(\tau)$
U	—	21.9	26.1	—	21.9	26.0	—	11.9	9.1
L	7.25	11.0	52.2	7.16	10.9	51.2	2.38	4.6	9.8
T	—	5.1	—	—	5.1	—	—	3.0	—
I	—	8.8	—	—	8.8	—	—	4.5	—
P	—	−19.0	−25.2	—	−18.9	−25.1	—	−10.1	−8.7
A	—	−5.4	—	—	−5.4	—	—	−2.6	—
$\tilde{U}$	—	—	—	—	0.01	0.03	—	1.4	1.4
$\tilde{L}$	—	—	—	0.02	0.02	0.18	0.33	0.6	1.8
$\tilde{T}$	—	—	—	—	0.002	—	—	0.3	—
$\tilde{I}$	—	—	—	—	0.01	—	—	0.5	—
$\tilde{S}$	—	—	—	0.05	0.04	0.55	1.10	0.8	5.3
$\tilde{S}L$	—	—	—	0.02	0.02	0.18	0.35	0.4	1.7
$\tilde{S}T$	—	—	—	—	0.01	—	—	0.3	—
Γ	7.25	32.9	78.3	7.23	32.8	78.0	3.82	19.2	27.4
$\langle P_L\rangle$	−1	−1	−1	−0.98	−1.0	−0.98	−0.25	−0.72	−0.38
α_{θ^*}	—	0.003	—	—	0.003	—	—	−0.11	—

transverse and parity-odd no-flip contributions U and P add destructively. That $P_L(B\to D) > P_L(b\to c) > P_L(B\to D^*)$ over the whole y-range reflects the relative strength of flip and no-flip contributions as evidenced by the partial rates in Table 1.

Next we turn to the s.l. $B\to\pi(\rho)$ and $b\to u$ decays involving the $b\to u$ transition. As our model parameters we take $m_{FF} = m_{Bu^*} = 5.33\,\text{GeV}$ and $I_{bu} = 0.33$ as suggested by [2]. Further we choose $m_b = 4.73\,\text{GeV}$ and $m_u = 0.3\,\text{GeV}$.

In Table 2 we list our pedictions for the $b\to u$ transitions. When comparing the exclusive $B\to\pi$ and $B\to\rho$ modes with the FQD modes one has to take into account the theoretical uncertainty in the calculation of the overlap factor I_{bu} which could easily deviate from its value of $I_{bu} = 0.33$ used in this calculation by 25%. For this reason we limit our discussion to the qualitative features of the two exclusive $b\to u$ decay modes.

The total decay rates are generally reduced going from the e- to the τ-mode. The reduction, however, is not as strong as in the corresponding $b\to c$ transitions. The τ-rates are 52%, 58% and 34% of the corresponding e-rates in the $B\to\pi$, $B\to\rho$ and $b\to u$ cases, respectively. In the τ-mode the two decay channels $B\to\pi$ and $B\to\rho$ almost saturate the FQD rate. The flip rates are generally small except again for the scalar current contribution in the $B\to\pi$ cases which occurs at a level of 28% compared to the total rate. That the scalar current contribution is not as strong as in the $B\to D$ case discussed earlier is due to the fact that there is a strong cancellation of the F_+^V and F_-^V contributions to the scalar helicity amplitude H_T^π (with $F_+^V/F_-^V = -(M_1 - M_2)/(M_1 + M_2)\to -1$ as $M_2/M_1\to 0$) which partially compensates for the s-wave enhancement. The average longitudinal τ-polarization is negative for all three cases $B\to\pi$, $B\to\rho$ and $b\to u$. The largest reduction from the left-handed value $P_L = -1$ in the τ-mode occurs for the $B\to\pi$ cases with $P_L = -0.25$ which is mainly due to the strength of the scalar current contribution $\tilde{S}$. The alignment polarization of the ρ as measured by the asymmetry parameter α_θ^* is small for both e- and the τ-modes.

The $B\to\pi$, $B\to\rho$ and $b\to u$ hadron momentum spectra are shown in Fig. 14. In the e-mode the spectra rise to their highest values at $x = 1$ for $B\to\pi$ and $b\to u$. The $B\to\rho$ spectrum shows a shoulder around $x = 0.3$ at a lower x-value than in the corresponding $B\to D^*$ cases. This is due to the time-like form factor effect—the ρ prefers to be produced at low momentum where q^2 is largest. In the τ-mode all spectra become slightly softer which is due to the fact that the spectra go to zero at $x = 1$ in the τ-mode.

The $y\,(= p_l/p_{\max})$ lepton momentum spectra shown in Fig. 15 remain practically unchanged for the $B\to\pi$ case and become slightly softer for $B\to\rho$ and slightly harder for $b\to u$ when going from the e- to the τ-mode.

Figure 16 finally shows the y-independence of the longitudinal polarization. As in the corresponding

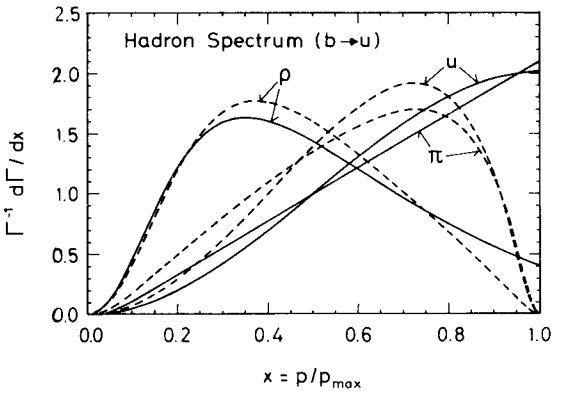

Fig. 14. $x\,(p/p_{\max})$ hadron momentum spectra of $b\to u(e)$ transitions (full lines and $b\to u(\tau)$ transitions (dashed lines)

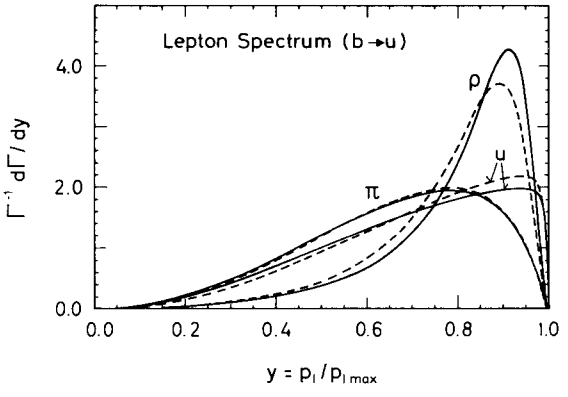

Fig. 15. $y\,(= p_l/p_{l\max})$ lepton momentum spectra of $b\to u(e)$ transitions (full lines) and $b\to u(\tau)$ transitions (dashed lines)

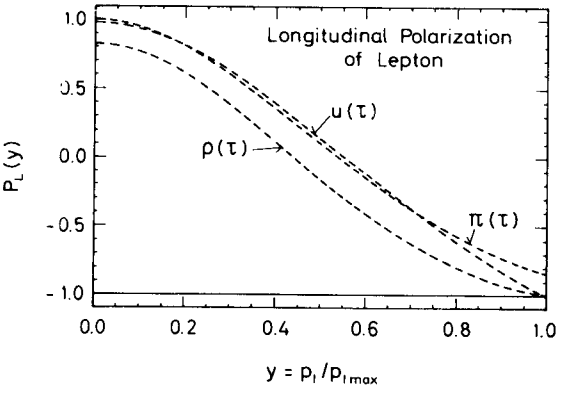

Fig. 16. $y\,(= p_l/p_{l\max})$ lepton momentum dependence of longitudinal polarization of the e and τ in $b\to u$ transitions

$b\to c$ transitions the flip contributions dominate at lower y-values whereas no-flip contributions dominate at higher y-values leading to positive and negative values of P_L at lower and higher y-values. The dominance of the respective contributions is, however, more pronounced than in the $b\to c$ transitions with $P_L(y=0)\cong +1$ and $P_L(y=1)\cong -1$ in all three cases.

Finally we discuss the s.l. $c \to s$ transitions $D \to K(K^*) + l^+ + \nu_l$ and the FQD $c \to s + l^+ + \nu_l$. For the overlap integral we take $I_{cd} = 0.82$ as in [2]. As form factor pole mass we take $m_{FF} = m_{D_s^*} = 2.11\,\text{GeV}$ for the monopole form factor. For the dipole form factor we choose a generalized vector dominance model (GVDM) form factor behaviour:

$$F(q^2) = F(0)\left[\frac{m_{FF}^2}{m_{FF}^2 - q^2} \cdot \frac{m_{FF}'^2}{m_{FF}'^2 - q^2}\right]$$
$$= F(0)\left[\frac{1}{m_{FF}^2 - q^2} - \frac{1}{m_{FF}'^2 - q^2}\right]\frac{m_{FF}^2 m_{FF}'^2}{m_{FF}'^2 - m_{FF}^2} \qquad (60)$$

where $m_{FF}' = 2.71\,\text{GeV}$ is the mass of the first recurrence of the D_S^* according to the potential model approach of [34]. The GVDM form factor (60) is the appropriate physical representation of a dipole-type form factor which, for reasons of simplicity, was chosen to be of the simple yet unphysical monopole squared form in the $b \to c$ and $b \to u$ cases (see (35)). For the quark masses occurring in the s.l. free quark decay we choose $m_c = 1.55\,\text{GeV}$ and $m_s = 0.45\,\text{GeV}$.

In Fig. 17 we show the q^2-spectra of the three s.l. decays $D \to K(K^*)$ and $c \to s$ in the e- and in the μ-mode. One notes that the difference in the e- and μ-modes occurs mainly for low q^2-values where the effect of the threshold-type factor $(q^2 - \mu^2/q^2)^2$ is most prominent. Whereas the μ-mode is slightly suppressed relative to the e-mode for $D \to K^*$ and $c \to s$ over the entire q^2-range, the μ-mode slightly dominates the e-mode for $q^2 > 0.15\,\text{GeV}^2$ in the s.l. $D \to K$ decay. The latter effect is again due to the relatively strong scalar current excitation in the μ-mode.

This is quite apparent in the values of the integrated partial rates listed in Table 3. The scalar flip contribution $\tilde{S}$ makes up 6.3% of the s.l. $D \to K(\mu)$ rate. The scalar flip contribution is less pronounced with 2.5% and 4.6% in the $D \to K^*(\mu)$ and $c \to s(\mu)$ decays respectively. In all three cases the strongest rate reduction occurs for the longitudinal no-flip contribution L when going from the e- to the μ-modes. This is easy to understand since it is the longitudinal mode which is most strongly affected by the threshold factor $((q^2 - \mu^2)/q^2)^2$ as Fig. 18 shows.

Table 3 shows a slight dominance of the s.l. $D \to K$ rate over the $D \to K^*$ rate where the ratio of rates in the e-mode is calculated as $R = \Gamma^{\text{s.l.}}_{D \to K^*}/\Gamma^{\text{s.l.}}_{D \to K} = 0.96$. This is considerably smaller than the corresponding ratio ($\simeq 3$) found in B decays discussed earlier in this section. The relatively large K-rate can partly be understood as a timelike form factor effect: the available time-like q^2-range is quite close to the relevant $(c\bar{s})$ form factor pole with form factor mass $m_{D_s^*} \simeq 2.11\,\text{GeV}$. This is further illustrated by listing the maximal q^2-values for the s.l. decay cases $(D \to K^*, D \to K)$ and $(B \to D^*, B \to D)$ which are $(0.96, 1.9\,\text{GeV}^2)$ and $(10.7, 11.6\,\text{GeV}^2)$. The corresponding form factor poles are at $q^2 = 4.45\,\text{GeV}^2$ and $40.2\,\text{GeV}^2$ for the $c \to s$ and $b \to c$ cases.

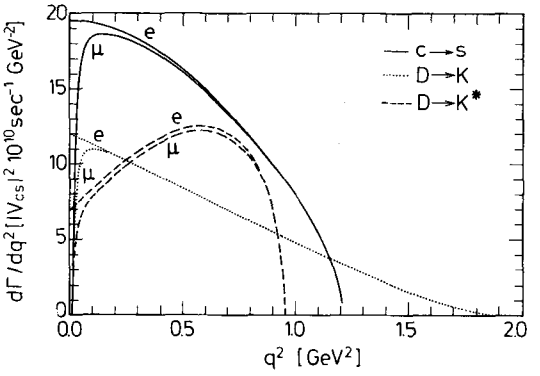

Fig. 17. q^2-spectra of s.l. decay rates $D^+ \to K^o + l^+ + \nu_l$ (dotted), $D^+ \to K^{*o} + l^+ + \nu_l$ (dashed) and $c \to s + l^+ + \nu_l$ (full)

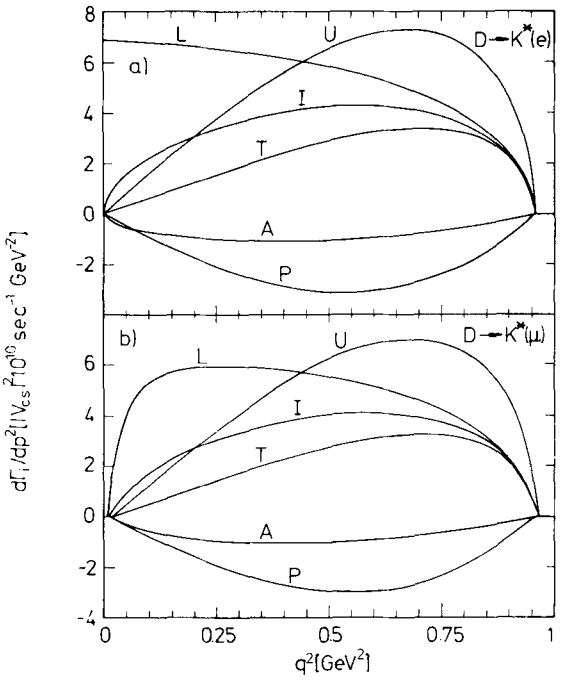

Fig. 18 a, b. Partial helicity rates $d\Gamma_i/dq^2$, $i = U, L, T, I, P, A$ as functions of q^2 for $D^+ \to K^{*o} + l^+ + \nu_l$ with $l = e$ **a** and $l = \mu$ **b**. Flip rates $d\tilde{\Gamma}_i/dq^2$ are not shown as they are tiny on the scale of the figure

Recently the s.l. rates have been measured to be $(8.2 \pm 1.2) \times 10^{10}\,\text{s}^{-1}$ and $(4.2 \pm 0.6 \pm 0.5) \times 10^{10}\,\text{s}^{-1}$ for $D \to K(e)$ and $D \to K^*(e)$, respectively (see [35]). Using $V_{cs} = 0.975$ and the numbers in Table 3 we find $9.7 \times 10^{10}\,\text{s}^{-1}$ and $9.3 \times 10^{10}\,\text{s}^{-1}$ for the two rates. Whereas the $D \to K$ rate can be accounted for in our approach, the $D \to K^*$ rate comes out too large. A further disagreement with the $D \to K^*$ measurement occurs for the ratio of the longitudinal to the unpolarized transverse contribution. We find $L/U = 1.1$ in the e-mode whereas the measurement of E691 has a stronger longitudinal component, cif. $L/U = 2.4^{+1.7}_{-0.9} \pm 0.2$ [34]. If the results of the E691 $D \to K^*$ measurements are confirmed by other experiments the present simple spectator quark model would require some more fine-tuning, at least in the $c \to s$ sector.

Table 3. Partial rates, total rates and polarization parameters for s.l. $c \to s$ transitions in the e- and μ-sectors. $m_c = 1.55\,\text{GeV}$ and $m_s = 0.45\,\text{GeV}$. Rates in units of $|V_{cs}|^2\ 10^{10}\,\text{s}^{-1}$

	$D \to K(e)$	$D \to K^*(e)$	$c \to s(e)$	$D \to K(\mu)$	$D \to K^*(\mu)$	$c \to s(\mu)$
U	—	4.7	5.5	—	4.4	5.2
L	10.2	5.2	11.0	9.1	4.5	9.5
T	—	2.1	—	—	2.0	—
I	—	3.2	—	—	2.9	—
P	—	−2.0	−3.7	—	−1.9	−3.5
A	—	−0.8	—	—	−0.7	—
$\tilde{U}$	—	—	—	—	0.06	0.06
$\tilde{L}$	—	—	—	0.2	0.10	0.2
$\tilde{T}$	—	—	—	—	0.02	—
$\tilde{I}$	—	—	—	—	0.05	—
$\tilde{S}$	—	—	—	0.6	0.2	0.7
$\tilde{S}L$	—	—	—	0.2	0.09	0.2
$\tilde{S}T$	—	—	—	—	0.04	—
Γ	10.2	9.8	16.5	9.9	9.3	15.7
$\langle P_L \rangle$	1	1	1	0.84	0.92	0.87
α_{θ^*}	—	1.21	—	—	1.17	—

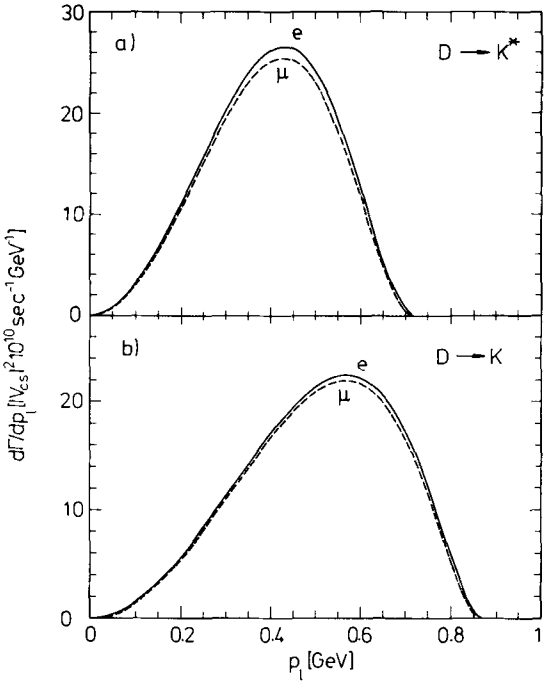

Fig. 19 a, b. Lepton momentum spectrum for **a** $D^+ \to K^{*o} + l^+ + \nu_l$ and **b** $D^+ \to K^o + l^+ + \nu_l$ for $l = e$ (full) and $l = \mu$ (dashed)

Figure 19 shows the lepton mass effect on the lepton momentum spectrum in the $D \to K(K^*)$ decays. The differential rate becomes uniformly reduced in both the $D \to K$ and $D \to K^*$ decays, where the reduction is larger in the $D \to K^*$ case. This is reflected in the total rates listed in Table 3 where one finds $\Gamma_{B \to D^*(\mu)}/\Gamma_{B \to D^*(e)} = 0.95$ and $\Gamma_{B \to D(\mu)}/\Gamma_{B \to D(e)} = 0.97$. These observations imply slightly softer endpoint spectra in the μ-modes where the effect is stronger in the $D \to K^*$ mode (see Fig. 19).

7 Summary and conclusions

We have presented a detailed analysis of lepton–hadron correlations in exclusive semi-leptonic decays including lepton mass effects.

In the (2 hadron-2 lepton) case relevant to the s.l. decays $B \to D^*$ and $b \to c$ one has the familiar (3 + [2])-fold structure where the number in the square bracket refers to the added structure when lepton mass effects are included.* In the (3 hadron-2 lepton) case relevant to the the cascade decay $B \to D^*(\to D\pi) + l^- + \bar{\nu}_l$ one has the familiar (6 + [3])-fold structure which would be appended by an additional (3 + [1]-fold structure if T-odd or CP-odd effects would be included which were not discussed in this paper.

Our discussion centered on the quark transitions $Q \to q$. The corresponding antiquark transition cases $\bar{Q} \to \bar{q}$ can easily be included within the formalism of this paper by noting that the transverse helicity amplitudes are related by $H^{\pm}(\bar{Q} \to \bar{q}) = (H^{\mp}(Q \to q)$ whereas the longitudinal and scalar helicity amplitudes remain unchanged. This only effects the p.v. structure functions $\hat{H}_P$ and $\hat{H}_A$ whose sign change.

We have used a simple spectator quark model (the KS model) for the s.l. $B \to D(D^*)$, $B \to \pi(\rho)$ and $D \to K(K^*)$ decays to calculate the various structure functions relevant to these exclusive s.l. decays. We discussed rates, spectra, angular distributions and the longitudinal polarization of the lepton that can be measured in these s.l. decay processes. We worked out in detail how lepton mass effects effect these observables.

* In the $B \to D$ case this reduces to a (1 + [2])-fold structure because the spin 0 − spin 0 transitions does not allow for a transverse contribution

We concluded that the s.l. $B \to D$ and $B \to \pi$ decays are more sensitive to lepton mass effects than the s.l. $B \to D^*$ and $B \to \rho$ decays due to a strong scalar current excitation in the former case. This would allow one to experimentally isolate the new dynamics brought in by the invariant scalar form F_-^V in the s.l. $B \to D(\tau)$ decays. A determination of the corresponding new scalar form factor F_3^A in the s.l. $B \to D^*(\tau)$ and $B \to \rho(\tau)$ appears to be more difficult.

The angular distribution structure discussed in this paper together with the associated structure functions calculated in this paper within the context of the KS model can be used as input in efficient Monte Carlo generator programs that are needed to do reliable acceptance corrections to experimental decay distributions.

Let us conclude with an optimistic note. Present plans for next generation B-factories call for a yearly rate of $10^7 - 10^8$ analyzed B-meson decays necessary to discover possible CP-violating effects in B-meson decays. Such a large yearly sample of B-meson decays would provide ample opportunity to experimentally measure the various observables discussed in this paper.

Acknowledgements. Part of this work was done while one of us (J.G.K.) was a visitor at the DESY theory group. J.G.K. would like to thank the theory group for hospitality and the DESY directorate for support.

Appendix A

Decay kinematics

We are dealing with a one → three particle decay with momenta (masses) $p_1(M_1) \to p_2(M_2) + l(\mu) + l'(0)$. The decay kinematics of such processes is well documented (see e.g. [36]). There are two independent kinematic variables. In our discussion we shall use the two complimentary sets (i) $q^2, \cos\theta$ and (ii) q^2, E_l, where q^2 is the momentum transfer squared, E_l is the lepton's energy in the B rest system and θ is the polar angle of the lepton in the lepton–neutrino rest system as defined in Fig. 1.

The bounds on q^2 are given by

$$\mu^2 \leqq q^2 \leqq (M_1 - M_2)^2 \tag{A1}$$

where the lower and upper bound correspond to the D momentum being maximal

$$p_{\max} = (M_1^4 + M_2^4 + \mu^4 - 2M_1^2M_2^2 - 2M_1^2\mu^2 - 2M_2^2\mu^2)^{1/2}/2M_1 \tag{A2}$$

and minimal ($p = 0$). The bounds for the lepton energy are given by

$$\mu \leqq E_l \leqq \frac{M_1^2 - M_2^2 + \mu^2}{2M_1} \tag{A3}$$

where the lower and upper bound correspond to the lepton's momentum being minimal ($p_l = 0$) and maximal ($p_{l\max} = p_{\max}$) (see (A2)), respectively. For the cosine of the scattering angle θ one has

$$\cos\theta = \frac{(M_1^2 - M_2^2 + q^2)(q^2 + \mu^2) - 4q^2M_1E_l}{2M_1p(q^2 - \mu^2)} \tag{A4}$$

$\cos\theta = \pm 1$ defines the phase space boundaries in the (q^2, E_l)-plane as shown in Figs. 2 and 3. One has

$$E_l^{\pm} = \frac{1}{2M_1}\left[q^2 + \mu^2 - \frac{1}{2q^2}((q^2 - M_1^2 + M_2^2)(q^2 + \mu^2) \mp 2M_1p(q^2 - \mu^2))\right]. \tag{A5}$$

The calculation of the lepton energy spectrum requires the integratic limits $q_{\pm}^2 = q_{\pm}^2(E_l)$, i.e. the inverse of (A5).

One obtains

$$q_{\pm}^2 = \frac{1}{a}(b \pm \sqrt{b^2 - ac}) \tag{A6}$$

where

$$a = M_1^2 + \mu^2 - 2M_1E_l$$
$$b = M_1E_l(M_1^2 - M_2^2 + \mu^2 - 2M_1E_l) + \mu^2M_2^2$$
$$c = \mu^2[(M_1^2 - M_2^2)^2 + \mu^2M_1^2 - (M_1^2 - M_2^2)2M_1E_l].$$

Appendix B

Derivation of angular decay distribution

Our aim is to expand the lepton tensor $L_{\mu\nu}$ into a complete set of covariant helicity vectors. This can be achieved by using the completeness relation (6). Consider the lepton–hadron correlation function $L^{\mu\nu}H_{\mu\nu}$. Using the completeness relation (6) $L^{\mu\nu}H_{\mu\nu}$ can be written as

$$L^{\mu\nu}H_{\mu\nu} = L_{\mu'\nu'}g^{\mu'\mu}g^{\nu'\nu}H_{\mu\nu} = \sum_{\substack{mm' \\ nn'}} (L_{\mu'\nu'}\bar{\varepsilon}^{\mu'}(m)\bar{\varepsilon}^{\nu'*}(n)g_{mm'}g_{nn'})\bar{\varepsilon}^{\mu*}(m')\bar{\varepsilon}^{\nu}(n')H_{\mu\nu}. \tag{B1}$$

The expression in brackets in (B1) provides the desired expansion coefficients for the expansion of $L^{\mu\nu}$ into the tensor basis $\bar{\varepsilon}^{\mu*}(m)\ \bar{\varepsilon}^{\nu}(m')$.

The point is that the two Lorentz contractions appearing on the r.h.s. of (B1) can be evaluated in two different Lorentz systems. The bracketed expression will be evaluated in the $(l\bar{\nu})$ CM system bringing in the decay angles θ and χ as drawn in Fig. 1, whereas the remaining part will be evaluated in the B rest system bringing in the helicity amplitudes as defined in Sect. 2. Turning to the $(l\bar{\nu})$ CM system one has for the lepton momenta (see Fig. 1)

lepton:

$$l_\mu = (E_l, p_l\sin\theta\cos\chi, p_l\sin\theta\sin\chi, p_l\cos\theta)$$

antineutrino:

$$l'_\mu = (p_l, -p_l\sin\theta\cos\chi, -p_l\sin\theta\sin\chi, -p_l\cos\theta)$$

with $E_l = (q^2 + \mu^2)/2\sqrt{q^2}$ and $p_l = (q^2 - \mu^2)/2\sqrt{q^2}$. The longitudinal and time-like polarization four-vectors are given by $\bar{\varepsilon}_\mu(0) = (0,0,0,-1)$ and $\bar{\varepsilon}_\mu(t) = (1,0,0,0)$ whereas the transverse parts remain unchanged from (3).

The expansion of the lepton tensor can be written very compactly in terms of Wigner d-functions. One has

$$L_{\mu\nu}(\theta,\chi) = \frac{1}{8} \sum_{\substack{\lambda_l \\ m,m' \\ J,J'}} (-1)^{J+J'} |h_{\lambda_l;\lambda_{l'}=\frac{1}{2}}|^2 e^{-im\chi} d^J_{m,\lambda_l - 1/2}(\pi - \theta) \cdot e^{im'\chi} d^{J'}_{m',\lambda_l - 1/2}(\pi - \theta) \bar{\varepsilon}^*_\mu(m) \bar{\varepsilon}_\nu(m'). \quad \text{(B2)}$$

The sum over J, J' runs over 0 and 1, and the indices m, m' run over the four components $\pm, 0$ and t. The terms $(J;m) = (1;0,\pm)$ and $(J';m') = (0;t)$, and $(J;m) = (0;t)$ and $(J';m') = (1;0,\pm)$ take care of the scalar-vector interference contributions $\hat{H}_{SL}$ and $\hat{H}_{ST}$ in (18) and (22). These terms obtain an extra phase from the factor $(-1)^{J+J'}$ coming from the metric factors $g_{mm'} g_{nn'}$ in (B1). The arguement of the Wigner functions is $(\pi - \theta)$ due to the "backward" definition of the z-axis (see Fig. 1). For the same reason one has $\chi \to -\chi$ compared to the standard decay formula.

The lepton helicity amplitudes $h_{\lambda_l;\lambda_{\bar{\nu}}=1/2}$ has been specified to the decay $B \to D^* + l^- + \bar{\nu}_l$ with positive helicity for the antineutrino. For the moduli squared of the lepton-side helicity amplitudes one calculates in the $(l^- \bar{\nu}_l)$ CM systems:

$$\text{spin no-flip:} \quad \lambda_l = -\tfrac{1}{2}: |h_{-1/2;1/2}|^2 = 8(q^2 - \mu^2)$$

$$\text{spin flip:} \quad \lambda_l = \tfrac{1}{2}: |h_{1/2;1/2}|^2 = 8\frac{\mu^2}{2q^2}(q^2 - \mu^2). \quad \text{(B3)}$$

The case $B \to D^* + l^+ + \nu_l$ involving a neutrino can be discussed along similar lines. The net effect is to change the sign of the angular coefficients multiplying the p.v. contributions $\hat{H}_P$ and $\hat{H}_A$ as indicated in (22).

In the same vein we can expand the strong decay tensor $Z_{\alpha\beta}$ describing the angular dependence in the decay $D^* \to D\pi$. One has

$$Z_{\alpha\beta}(\theta^*,\chi^*) = \frac{3}{2} \frac{M_2^2}{(p_2 p_3)^2 - M_2^2 M_3^3} p_3^{\alpha'} p_3^{\beta'} \varepsilon_{\alpha'}(m) \varepsilon^*_\beta(n) \cdot \varepsilon^*_\alpha(m') \varepsilon_\beta(n') \delta_{mm'} \delta_{nn'} \quad \text{(B4)}$$

where the invariant Lorentz contraction on the rhs of (B4) can now be evaluated in the D^* rest frame. As Fig. 1 shows we have chosen a system with $\chi^* = 0$. We can then write (B4) in terms of Wigner d-functions as

$$Z_{\alpha\beta}(\theta^*,\chi^* = 0) = \frac{3}{2} \sum_{m,m'} d^1_{om}(\theta^*) d^1_{om'}(\theta^*) \varepsilon^*_\alpha(m) \varepsilon_\beta(m'). \quad \text{(B5)}$$

The lepton and hadron decay functions (B2) and/or (B5) can then be used to evaluate the decay distributions $L^{\mu\nu}(\theta) H_{\mu\alpha}$ and $L^{\mu\nu}(\theta,\chi) H_{\mu\alpha;\nu\beta} Z^{\alpha\beta}(\theta^*)$ leading to the angular decay distributions (18) and (22). The advantage of using the covariant expansions (B2) and (B5) is that one can explicitly check on the phases component-wise without having to rely on a particular set of phase conventions.

References

1. Levman et al. CUSB Coll.: Phys. Lett. 141B (1984) 271; S. Behrends et al. CLEO Coll.: Phys. Rev. Lett. 59 (1987) 407; H. Albrecht et al. ARGUS Coll.: Phys. Lett. 197B (1987) 452; ibid 219B (1989) 121; K. Wachs Crystal Ball Coll.: DESY Preprint 87-084 (1987)
2. M. Wirbel, B., B. Stech, M. Bauer: Z. Phys. C—Particles and Fields 29 (1985) 637
3. B. Grinstein, M.B. Wise, N. Isgur: Phys. Rev. Lett. 56 (1986) 298; N. Isgur, D. Scora, B. Grinstein, M.B. Wise: Phys. Rev. D39 (1989) 799
4. A. Ali, J.G. Körner, G. Kramer, J. Willrodt: Z. Phys. C—Particles and Fields 1 (1979) 269; J.G. Körner in: Proceedings of the International Symposium on Production and Decay of Heavy Hadrons. Heidelberg 1986
5. J.G. Körner, G.A. Schuler: Z. Phys. C—Particles and Fields 38 (1988) 511
6. P.R. Auvil, J.J. Brehm: Phys. Rev. 145 (1966) 1152
7. R.P. Nabavi, X.Y. Pham, W.N. Cottingham: J. Phys. G11 (1977) 1485
8. J.L. Cortes, X.Y. Pham, A. Tounsi: Phys. Rev. D25 (1982) 188
9. F. Hussain, J.G. Körner, R. Migneron: to be published
10. S.J. Brodsky, G.P. Lepage: Phys. Rev. D22 (1980) 2157
11. A. Ali, T.C. Yang: Phys. Lett. 65B (1976) 275
12. I. Hinchcliffe, C.H. Llewellyn-Smith: Nucl. Phys. B114 (1976) 45
13. G.L. Kane: Phys. Lett. B70 (1977) 227
14. W.J. Wilson: Phys. Rev. D16 (1977) 742
15. V. Barger, T. Gottschalk, R.J.N. Phillips: Phys. Rev. D16 (1977) 746
16. F. Bletzacker, M.T. Nieh, A. Soni: Phys. Rev. D16 (1977) 732
17. X.Y. Pham, J.M. Richard: Nucl. Phys. B128 (1978) 453
18. M.B. Gavela: Phys. Lett. B83 (1979) 367
19. M. Suzuki: Phys. Lett. B155 (1985) 112, Nucl. Phys. B258 (1985) 553
20. S.-C. Chao et al.: Phys. Rev. D31 (1985) 1756; G. Kramer, W.F. Palmer: Phys. Rev. D36 (1987) 154; G. Kramer, W.F. Palmer: Z. Phys. C—Particles and Fields 39 (1988) 423; J.M. Cline, W.F. Palmer, G. Kramer: Phys. Rev. D40 (1989) 793
21. F. Schöberl, H. Pietschmann: Europhys. Lett. 2 (1986) 583
22. T. Altomari, L. Wolfenstein: Phys. Rev. Lett. 58 (1987) 1563
23. S. Nussinov, W. Wetzel: Phys. Rev. D36 (1987) 130
24. M. Bauer, M. Wirbel: Z. Phys. C—Particles and Fields 42 (1989) 671
25. C.A. Dominguez, N. Paver: Phys. Lett. B207 (1988) 499; Z. Phys. C—Particles and Fields 41 (1988) 217
26. P. Heiliger, L.M. Sehgal: Phys. Lett. 229B (1989) 409
27. J.G. Körner, G.A. Schuler: Phys. Lett. B226 (1989) 185
28. J.G. Körner, G.A. Schuler: Phys. Lett. 231B (1989) 306
29. K. Hagiwara, A.D. Martin, M.F. Wade: Phys. Lett. B288 (1989) 144 and to be published in Z. Phys. C—Particles and Fields
30. H. Albrecht et al. ARGUS Coll.: Phys. Lett. 291B (1989) 121
31. R. Gläser ARGUS: Talk given at Heavy quark symposium. Cornell, Ithaca (1989)
32. N. Katayama CLEO: Talk given at Heavy quark symposium. Cornell, Ithaca (1989)
33. H. Albrecht et al. ARGUS: Phys. Lett. 197B (1987) 452
34. S. Godfrey, N. Isgur: Phys. Rev. D32 (1985) 189
35. R.J. Morrison, M.S. Witherell: D-Mesons. UCSB-HEP-89-01 (1989), to be published in Ann. Rev. Nucl. Part. Sci. 39
36. E. Byckling, K. Kajantie: Particle kinematics. London, New York, Sydney, Toronto: Wiley 1973